General Disclaimer

One or more of the Following Statements may affect this Document

- This document has been reproduced from the best copy furnished by the organizational source. It is being released in the interest of making available as much information as possible.

- This document may contain data, which exceeds the sheet parameters. It was furnished in this condition by the organizational source and is the best copy available.

- This document may contain tone-on-tone or color graphs, charts and/or pictures, which have been reproduced in black and white.

- This document is paginated as submitted by the original source.

- Portions of this document are not fully legible due to the historical nature of some of the material. However, it is the best reproduction available from the original submission.

DRA 9/81

NUMERICAL ANALYSIS OF TURBULENT COAXIAL FLOW WITH INTERNAL HEAT GENERATION

Avi Lin* and Herbert Weinstein

Department of Chemical Engineering
The City College of the
City University of New York
New York, New York 10031

This research was supported by
NASA Grant NSG-3174

January 1981

---

* Present Address: Department of Aerospace Engineering and Applied Mechanics, University of Cincinnati, Cincinnati, Ohio 45221.

TABLE OF CONTENTS

SUMMARY

This work outlines an upwind, second order accuracy, coupled, conservative numerical scheme for solving a two dimensional laminar or turbulent flow field. Mean vorticity, ω, and mean stream function, ψ, are used as the mean flow dependent variables. The turbulent kinetic energy k and the turbulent energy decay rate, ε, are used to define the turbulence state. The rate of convergence of the coupled, conservative, mean field system ψ-ω as well as the turbulence state system k-ε, is twice that realized when solving these equations separately. Although the turbulence boundary conditions have a non-regular variation near a solid wall, the turbulence model is reduced exactly to this variation, keeping the conservative features.

The axisymmetric mixing of two confined jets with an internal heat source is considered with this numerical scheme. The inlet boundary conditions have a limited effect if they are applied far upstream of the end of the inner cylinder (~ 5 radii). The fully developed flow conditions which apply at the exit section, should be located far downstream to prevent an effective change in the real flow Reynolds number. The parabolic conditions at the exit section are found to be very good. A laminar recirculation zone appears f r certain flow parameters whose length tends to some asymptotic value as the Reynolds number increases. During the variation of the Reynolds number, the recirculation mass flux approaches a maximum. Thermal radiation from the heat generating inner jet material is the leading mechanism of thermal

energy generating transport. This transport does not appear to depend heavily on the turbulent diffusion coefficients. The temperature field depends mainly on the radiative conductivity coefficients and on the heat generation. The latter is the only term that depends on the turbulence status through the species concentrations. The conditions for obtaining stable turbulent flow solutions are stated in this study, and are, almost always, fulfilled.

1. INTRODUCTION

Computational methods, as a tool to analyze physical phenomena and to solve the related engineering problems, are becoming even more popular today. This is mainly due to the rapid growth in computer capability (in terms of direct access memory and the improvement in the CPU time per elementary action) and improvements in the basic numerical schemes.

This report concentrates on developing computational method with which to obtain a physical understanding of the turbulent field of two coaxial jets entering an axisymmetric chamber. Even the laminar field of this flow is quite complicated. This is due to the many different domains which exist in the field especially in the entrance region. Physically, three regions may be identified: the wall region, the initial region near the axis of symmetry and the mixing region. Advancing downstream, these regions change relative size with the ratio of the two jets' mass fluxes as the main parameter. The turbulent field of these flows is much more complicated due to the difference in the effective transport coefficients and turbulence level from region to region. However, being aware beforehand of the complications and the different regions of this field, one can adjust the appropriate turbulence model and numerical scheme to treat the problem.

The objective of the present study is to describe numerically the velocity, concentration and temperature fields in confined coaxial turbulent flows with internal energy generation.

Physically, the flow system considered has an inner flow which is slower and heavier than the outer flow. The inner flow material undergoes nuclear fission in the chamber cavity and generates heat. This system is representative of a gas core nuclear reactor where the inner gas is fissionable and the outer flow is some lighter working fluid. The resultant flow is usually turbulent. In applying a turbulent model to a flow one has to compromise between choosing a high order of closure and paying in an extremely complex code for computing the phenomena, and choosing a very simple algebraic model and paying in a poor prediction of the phenomena. In this study the "two equation" model of the type k-ε[1] (k is the turbulence level and ε is the turbulence dissipation) was adopted, since, as has been stated in the literature[2], it is the closest-to-optimal model to predict two dimensional elliptic fluid flows available today. Both k and ε are governed by convection-diffusion like equations. Once k and ε are known at every point in the field, the effective transport coefficients can be calculated with models for the turbulent Prandtl and Schmidt numbers. Since the rate of energy generation in the core is very high, very high temperatures occur. Therefore thermal radiation is the dominant mechanism of energy transport (and the conductive transport is not negligible). In such a case it is very convenient to apply the Rosseland energy diffusion approximation.[3] This approximation, which is valid only for flows with high absorptivity results in a radiative conductivity like term in the equations.

The following variables define the two dimensional axi-symmetric field:

2	velocity components (u,v)
2	turbulent state variables (k,ε)
1	temperature variable (T)
1	pressure variable (P)
1	concentration variable (C)
7	variables

These variables are controlled by the following governing equations:

1	continuity
2	momentum
2	turbulence model
1	energy
1	species
7	equations

In the present field, as well as in many other fields it is very convenient to choose the stream function (ψ)-vorticity (ω) variables instead of the pressure (p)-velocity (u,v) variables, because the number of equations and unknowns is then reduced to six (6).

The numerical solution is performed on a non-uniform mesh grid that is spread over the domain of interest. The finite differences for all the terms are accurate to the second order, and unlike some other schemes[4,5], no artificial viscosity

is inserted and the flow is solved for the correct Reynolds number. In order to improve the stability, the equations are solved with as much coupling as is possible. The flow field equations (ψ-ω) are solved in a coupled manner, as well as the turbulent variables (k-ε). The energy equation and the concentration equation are solved separately. The algebraic difference equations are solved iteratively by successive line relaxation [or generally, by the successive block line relaxation].

2. FORMULATION OF THE PROBLEM AND PHYSICAL ASSUMPTIONS

The flow system under consideration is sketched in Fig. 1.1. The system consists of two concentric cylinders, with the outer cylinder of diameter D_2 continuous to a distance L_2, and the inner cylinder of diameter $D_1 < D_2$, is continuous to a distance $L_1 < L_2$, and ends at the section A-A.

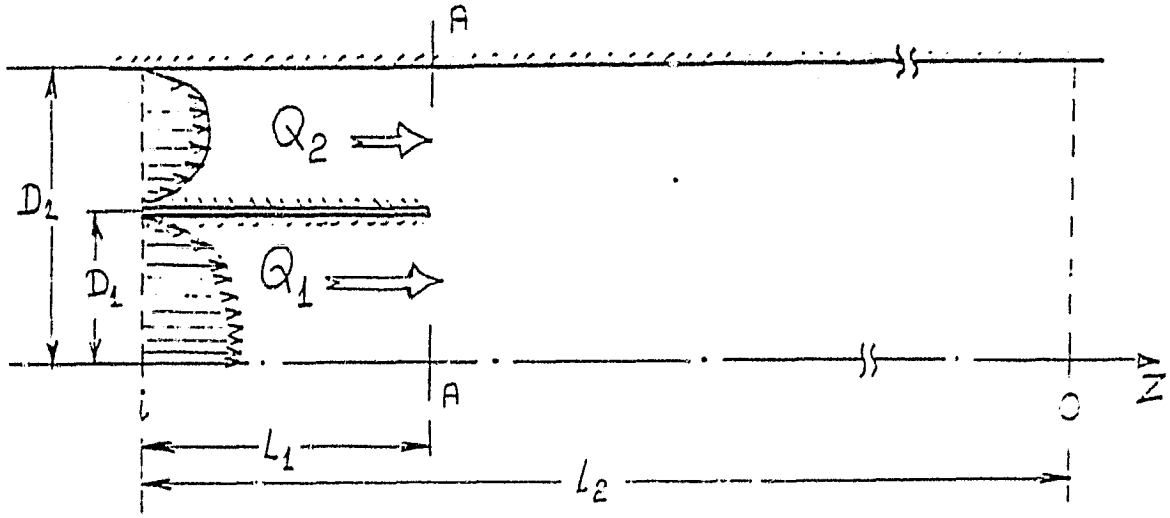

Fig. 1.1. Schematic Fields of the Physical Problem.

Different fluids with different mass fluxes and densities move through the inner cylinder (denoted with lower index 1) and through the annulus between the inner and the outer cylinder (denoted with lower index 2). Despite the simplicity of the flow system, complex physical processes take place, relating to the detachment of the stream from the inner cylinder trailing edge, contraction or expansion of the inner stream after the section A-A, and resulting for some cases in a recirculation region downstream

of the section A-A. Depending on the geometrical ratio D_1/D_2, the mass flux ratio Q_1/Q_2 and the laminar Reynolds number ratio, a recirculation zone can occur either on the axis of symmetry or on the outer cylindrical wall. There is also some weak dependence of this phenomenon on the upstream turbulent properties ratio. In order to describe the complexity of the physical processes occurring within the nozzle area in terms of the governing equations, these should be of the elliptic type.

In the subsequent part of this report, a mathematical model of the flow in this geometry will be presented. Let us begin with the following assumptions:

(i) The fluids are incompressible and of constant density.

(ii) A fully developed turbulent flow exists at the entrance to the computational region, a distance L_1 before the section A-A.

(iii) The flow properties are isothermal.

(iv) The duct walls are impermeable.

These assumptions will lead to a mathematical model of the flow field. With this model, described in the next section, it is possible to determine the velocity distribution in the computational domain as well as approximate the temperature and concentration distributions.

3. MATHEMATICAL MODEL OF THE FLOW FIELD

3.1 The Governing Transport Equations of the Flow

Steady, axially-symmetric flow of a viscous and incompressible gas with constant molecular transport coefficients is described by the equations of continuous media motion, namely the momentum equations coupled with the equation of continuity. These Navier-Stokes equations in cylindrical coordinates, r,z, are:[6]

continuity:

$$\frac{\partial u}{\partial z} + \frac{1}{r}\frac{\partial}{\partial r}(rv) = 0 \tag{3.1}$$

z-momentum:

$$\rho\left(u\frac{\partial u}{\partial z} + v\frac{\partial u}{\partial r}\right) = -\frac{\partial P}{\partial z} + \frac{1}{r}\frac{\partial}{\partial r}\left[r\,\mu_{eff}\left(\frac{\partial v}{\partial z} + \frac{\partial u}{\partial r}\right)\right] + 2\frac{\partial}{\partial z}\left(\mu_{eff}\frac{\partial u}{\partial z}\right) \tag{3.2}$$

r-momentum:

$$\rho\left(u\frac{\partial v}{\partial z} + v\frac{\partial v}{\partial r}\right) = -\frac{\partial P}{\partial r} + \frac{2}{r}\frac{\partial}{\partial r}\left(r\,\mu_{eff}\frac{\partial v}{\partial r}\right) - 2\,\mu_{eff}\frac{v}{r^2} + \frac{\partial}{\partial z}\left[\mu_{eff}\left(\frac{\partial v}{\partial z} + \frac{\partial u}{\partial r}\right)\right] \tag{3.3}$$

where u,v are the mean velocity components in the z and r directions, ρ is the density and p is the mean pressure. The quantity μ_{eff} appearing in the equations (3.2) and (3.3) is the so-called effective viscosity, being the sum of the molecular (laminar) viscosity μ_ℓ and the turbulent viscosity μ_t. It characterizes the turbulence status at a given point of the flow field:

$$\mu_{eff} = \mu_{\ell} + \mu_t \qquad (3.4)$$

A turbulent flow is thus treated like a laminar flow with a variable viscosity coefficient, which is characterized by special rations to the mean flow and other turbulence quantities. This relation is the main result of the turbulence model.

3.2 The Turbulence Model

A broad review of turbulence models is presented by Launder and Spalding.[7] The various models are classified according to their complexity and useability, which depend on the particular physical hypotheses employed to describe different turbulent fields. On the basis of physical analysis of the phenomena taking place in the field of the two coaxial flows, a "two equation" turbulence model is adopted as recommended in reference [2]. This model consists of two dynamic equations for two turbulence variables: the first equation is for the turbulent kinetic energy (k); and the second equation is for the dissipation (ε) of the turbulent energy.

The turbulent kinetic energy is defined by the half mean of the sum of the square of the turbulent velocity fluctuations:

$$k = \frac{1}{2} \overline{u_i'^2}$$

and the turbulent energy dissipation (or decay) is defined by

$$\varepsilon = \frac{1}{2} \overline{\left(\frac{\partial u_i'}{\partial x_j}\right)^2}$$

where in both formulations there is a tensorial summation over $1 \leq i, j \leq 3$, and u_i is the velocity fluctuation in the i direction. It can be seen that k and ε are positive definite quantities.

A general form of the k-ε model has been given by Launder and Spalding.[2] The transport equations for k and ε, in cylindrical coordinates are of the following form:

$$\rho\left(u \frac{\partial k}{\partial z} + v \frac{\partial k}{\partial r}\right) = \frac{\partial}{\partial z}\left(\frac{\mu_{eff}}{\sigma_k} \frac{\partial k}{\partial z}\right) + \frac{1}{r} \frac{\partial}{\partial r}\left(r \frac{\mu_{eff}}{\sigma_k} \frac{\partial k}{\partial r}\right) + \mu_{eff} G - \rho\varepsilon \tag{3.5}$$

$$\rho\left(u \frac{\partial \varepsilon}{\partial z} + v \frac{\partial \varepsilon}{\partial r}\right) = \frac{\partial}{\partial z}\left(\frac{\mu_{eff}}{\sigma_\varepsilon} \frac{\partial \varepsilon}{\partial z}\right) + \frac{1}{r} \frac{\partial}{\partial r}\left(r \frac{\mu_{eff}}{\sigma_\varepsilon} \frac{\partial \varepsilon}{\partial r}\right) + \frac{\varepsilon}{k}\left(C_1 \mu_{eff} G - C_2 \rho\varepsilon\right) \tag{3.6}$$

where the generation term is:

$$G = 2\left[\left(\frac{\partial u}{\partial z}\right)^2 + \left(\frac{\partial v}{\partial r}\right)^2 + \left(\frac{v}{r}\right)^2\right] + \left(\frac{\partial u}{\partial r} + \frac{\partial v}{\partial z}\right)^2 \tag{3.7}$$

knowing local values of k and ε one may determine local values of turbulent viscosity from the Prandtl and Kolmogorov[8] formula:

$$\mu_t = C_\mu \rho \frac{k^2}{\varepsilon} \tag{3.8}$$

The values of the constants appearing in equations (3.5), (3.6) and (3.8) for the turbulence model are suggested by Launder and Spalding[2] as follows:

$$C_1 = 1.44, \qquad C_2 = 1.92, \qquad C_\mu = 0.09$$

$$\sigma_k = 1.0, \qquad \sigma_\varepsilon = 1.3 \tag{3.9}$$

These values will be reviewed later on in this report.

3.3 The Energy and Species Equations

Since the flow field in the present study is incompressible, the Eckert number is zero and therefore the substantial derivatives of pressure may be ignored in the mean energy equation. In the absence of body forces the following energy equation may be considered:

$$\rho C_p \left[\frac{\partial}{\partial z}(ruT) + \frac{\partial}{\partial r}(rvT)\right] = \frac{\partial}{\partial z}\left[r\bar{\lambda}\frac{\partial T}{\partial z}\right] + \frac{\partial}{\partial r}\left[r\,\bar{\lambda}\frac{\partial T}{\partial r}\right] + \phi + S_T \tag{3.10}$$

where $\bar{\lambda}$ is the total thermal diffusivity, and ϕ is the dissipation given by

$$\phi = \mu_{eff}\left[2\left(\frac{\partial u}{\partial z}\right)^2 + 2\left(\frac{\partial v}{\partial r}\right)^2 + 2\left(\frac{v}{r}\right)^2 + \left(\frac{\partial u}{\partial r} + \frac{\partial v}{\partial z}\right)^2\right] \tag{3.11}$$

and is equal to the generation term of the turbulence energy given partially by eq. (3.7). Generally $\bar{\lambda}$ is given by

$$\bar{\lambda} = \lambda_\ell + \lambda_t + \lambda_r \tag{3.12}$$

where the first term on the right hand side of eq. (3.12) is the laminar contribution and the second term is the turbulent contribution to the thermal conductivity; λ_r stands for contributions

from other conduction-like processes. S_T in eq. (3.10) is the energy generation rate term, representing an energy source such as a chemical or nuclear reaction. In the present work we are interested especially in the effects of nuclear fission on the field's temperature. Regularly, the nuclear-reactive species enter the field through the inner pipe with concentration C, and the fission is carried out in the core of the field. The major mode of transfer of the nuclear energy is by radiation processes. According to some well defined physical models, like the Rosseland diffusion approximation[3] λ_r, which is a radiative conductivity coefficient, can have only a positive non-zero value, and the undimensional source term will be of the form

$$S = - \text{Arc} \left[1 - \frac{1}{2} \left(2 \frac{z}{L} - 1\right)^4\right] \tag{3.13}$$

where A is a constant and $L = L_1$ is the axial length of the chamber. The formula for λ_r is

$$\lambda_r = B\, T^3 \tag{3.14}$$

The values of the constants were taken to be[3]

$$B = \frac{32}{3\,\tau\beta} \quad , \quad A \approx 50.0 \tag{3.15}$$

where $\tau \approx 8$, $\beta \approx 400(°K)$ and the temperature T is measured in °K.

The equation of species continuity is taken similar in form to that of the energy equation since both temperature and concentration are scalar quantities. The difference is that the quantity C is not generated in or lost from the system.

This form of the species continuity equation is an approximation which is only good for small variations in density. However the simplification resulting from this assumption warrants its use in this illustrative development. The governing equation is then:

$$\frac{\partial}{\partial z}(ruc) + \frac{\partial}{\partial r}(rvc) = \frac{\partial}{\partial z}(r\bar{D}\frac{\partial c}{\partial z}) + \frac{\partial}{\partial r}(r\bar{D}\frac{\partial c}{\partial r}) \qquad (3.16)$$

where $\bar{D}$ is the total diffusion coefficient defined to be

$$\bar{D} = D_\ell + D_t \qquad (3.17)$$

where D_ℓ and D_t are the laminar and the turbulent diffusion coefficients.

3.4 The Dimensionless Form of the Equations

The parameters that control the flow field behavior can be found by casting the equations in dimensionless form. The velocities will be normalized with respect to the axial velocity component on the center line at the entrance section, U_o (see Fig. 3.1).

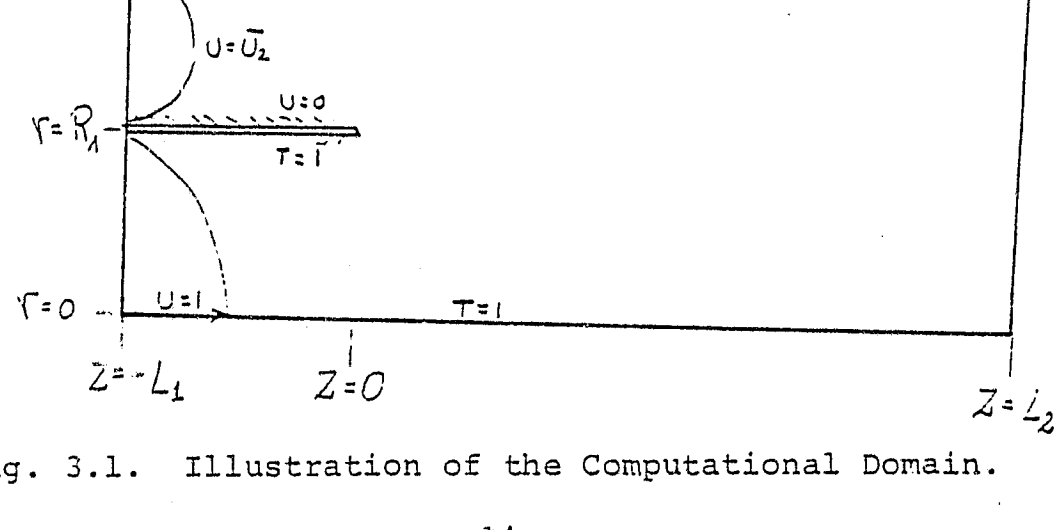

Fig. 3.1. Illustration of the Computational Domain.

The lengths are normalized with respect to the outer radius R_2. The temperature is normalized with respect to $\Delta T = T_0 - T_2$, where T_0 is the temperature at the centerline and T_2 is the outer cylinder wall temperature, both at the entrance section. The turbulence kinetic energy and the turbulent dissipation rate are normalized with respect to U_0^2 and U_0^3/D_2 respectively. (The pressure is normalized by ρU_0^2.) Therefore the flow field behavior is controlled by the following non-dimensional numbers:

Reynolds number: $Re = \frac{U_o D_2}{\nu}$

Laminar Prandtl number: $Pr = \frac{\mu_\ell C_p}{\lambda_\ell}$

Turbulent Prandtl number: $Pr_t = \frac{\mu_t C_p}{\lambda_t}$

Laminar Schmidt number: $Sc = \frac{\mu_\ell}{D_\ell}$

Turbulent Schmidt number: $Sc_t = \frac{\mu_t}{D_t}$

Eckert number: $E = \frac{U_0^2}{C_p \Delta T}$

Radiation number: $R_d = \frac{B}{\lambda_\ell^2} (°K)^2$

The following values for some of the above numbers will be adopted:

$Pr = 0.72, \quad Sc = 0.8$

$Pr_t = 1.0, \quad Sc_t = 1.0$

$E << 1$

$R_d >> 1 \ (20 \div 100)$

3.5 The Computation for an Incompressible Laminar Axisymmetric Flow

For an incompressible, laminar flow of a Newtonian fluid with constant viscosity in the absence of body forces, the axisymmetric Navier Stokes equations and the continuity equation (3.1 - 3.3), retaining the time term are:

$$\frac{\partial u}{\partial t} + v\frac{\partial u}{\partial r} + u\frac{\partial u}{\partial z} = -\frac{1}{\rho}\frac{\partial P}{\partial z} + \frac{1}{Re}\left(\frac{\partial^2 u}{\partial r^2} + \frac{\partial^2 u}{\partial z^2} + \frac{1}{r}\frac{\partial u}{\partial r}\right) \qquad (3.18a)$$

$$\frac{\partial v}{\partial t} + v\frac{\partial v}{\partial r} + u\frac{\partial v}{\partial z} = -\frac{1}{\rho}\frac{\partial P}{\partial r} + \frac{1}{Re}\left(\frac{\partial^2 v}{\partial r^2} + \frac{\partial^2 v}{\partial z^2} + \frac{1}{r}\frac{\partial v}{\partial r} - \frac{v}{r^2}\right) \qquad (3.18b)$$

$$\frac{\partial}{\partial r}(rV) + \frac{\partial}{\partial z}(rU) = 0 \qquad (3.18c)$$

These equations are referred to as the primitive variables equations since they are written in terms of the basic variables v, u and P. If the pressure is of primary importance in a particular incompressible field, the equations in this form plus the Poisson equation for pressure instead of the continuity equation (3.18c) should be considered.[9] Experience in solving these equations may also be useful if one is ultimately interested in three dimensional flows. Solution procedures for solving the primitive variable equations in both two- and three-dimensional rectangular coordinates are discussed by many investigators.[10,11] Since the pressure field is not of main interest in the present study, the following stream-function-vorticity formulation will be adopted.

By eliminating the pressure term in eqs. (3.18a) and (3.18b) by cross differentiation, applying eq. (3.18c) to this

result, and then using the definition of the vorticity ω:

$$\omega = \frac{\partial v}{\partial z} - \frac{\partial u}{\partial r} \tag{3.19}$$

the following dynamic equation for the vorticity may be obtained:

$$\frac{\partial \omega}{\partial t} + v \frac{\partial \omega}{\partial r} + u \frac{\partial \omega}{\partial z} - \frac{v\omega}{r} = \frac{1}{Re} \left[\frac{\partial^2 \omega}{\partial r^2} + \frac{\partial^2 \omega}{\partial z^2} + \frac{1}{r} \frac{\partial \omega}{\partial r} - \frac{\omega}{r^2}\right) \tag{3.20}$$

This "vorticity transport" form of the two dimensional Navier-Stokes equations can be modified by writing the continuity equation (3.18a) as:

$$\omega \frac{1}{r} \frac{\partial}{\partial r} (rv) + \omega \frac{\partial u}{\partial z} = 0$$

and adding it to the left hand side of eq. (3.20). Then the so-called "conservative form" of the vorticity transport equation is obtained:

$$\frac{\partial \omega}{\partial t} + \frac{\partial}{\partial r} (\omega v) + \frac{\partial}{\partial z} (\omega u) = \frac{1}{Re} \left(\frac{\partial^2 \omega}{\partial r^2} + \frac{\partial^2 \omega}{\partial z^2} + \frac{1}{r} \frac{\partial \omega}{\partial r} - \frac{\omega}{r^2}\right) \tag{3.21}$$

Introducing the incompressible stream function ψ defined by

$$\frac{1}{r} \frac{\partial \psi}{\partial r} = u \; ; \qquad \frac{1}{r} \frac{\partial \psi}{\partial z} = - v \tag{3.22}$$

into the continuity equation (3.18a) gives the following stream function-vorticity relation

$$\frac{\partial^2 \psi}{\partial r^2} + \frac{\partial^2 \psi}{\partial z^2} - \frac{1}{r} \frac{\partial \psi}{\partial r} + r\omega = 0 \tag{3.23}$$

Because the magnitudes of the stresses are often very important in the fluid field (they are, for example, responsible for

generating the turbulence), the components of the stress tensor for the incompressible axisymmetric flows studied here are of interest. These stresses in dimensionless form and in terms of velocity gradients and the laminar Reynolds number are:

$$\tau_{rr} = -\frac{2}{Re}\frac{\partial v}{\partial r}, \qquad \tau_{\theta\theta} = -\frac{2}{Re}\frac{v}{r}$$

$$\tau_{zz} = -\frac{2}{Re}\frac{\partial u}{\partial z}, \qquad \tau_{rz} = -\frac{1}{Re}\left(\frac{\partial u}{\partial r} + \frac{\partial v}{\partial r}\right) \tag{3.24}$$

Recent results for the two-dimensional driven-cavity problem indicate that convergence was more rapid with the ψ-ω formulation than with the primitive formulation that includes the pressure.[12] This study found that the accuracy of the primitive variable solution was very sensitive to the convergence tolerance used in solving for the pressure. Therefore the ψ-ω equations are used in this study to predict the flow field variables.

By substituting the vorticity given by eq. (3.23) into eq. (3.20), a single equation in terms of the stream function is obtained. This equation, called the "biharmonic equation", is:

$$\frac{\partial}{\partial t}(D^2\psi) - \frac{1}{r}\frac{\partial(\psi, D^2\psi)}{\partial(r,z)} - \frac{2}{r}\frac{\partial\psi}{\partial z}D^2\psi = \frac{1}{Re}D^4\psi \tag{3.25}$$

where the operators D^2 and D^4 are defined to be

$$D^2 = \frac{\partial^2}{\partial z^2} + \frac{\partial^2}{\partial r^2} - \frac{1}{r}\frac{\partial}{\partial r} \tag{3.26a}$$

and

$$D^4\psi = D^2(D^2\psi) \tag{3.26b}$$

Although the biharmonic equation contains only one unknown ψ, it is a fourth order nonlinear partial differential equation and is usually more difficult to solve. In [11] an efficient method of solving the steady planar biharmonic equation has been suggested. However, this solution method has poor convergence characteristics for a turbulent field, the two equations for the ψ-ω relations are considered hereafter.

Another minor variation of eq. (3.21) has also been used together with eq. (3.23). These forms differ only by the manner in which the diffusion term is written. For example, if in eq. (3.21) the

$$\frac{1}{r}\frac{\partial}{\partial r}\left(r\frac{\partial \omega}{\partial r}\right)$$

term is used instead of

$$\frac{\partial^2 \omega}{\partial r^2} + \frac{1}{r}\frac{\partial \omega}{\partial r} \quad ,$$

then, the following equivalent form is obtained:

$$\frac{\partial \omega}{\partial t} + \frac{\partial}{\partial r}(\omega v) + \frac{\partial}{\partial z}(\omega u) = \frac{1}{Re_R}\left[\frac{1}{r}\frac{\partial}{\partial r}\left(r\frac{\partial \omega}{\partial r}\right) - \frac{\omega}{r^2} + \frac{\partial^2 \omega}{\partial z^2}\right] \quad (3.27)$$

Really, there does not appear to be any significant advantage in using one of these equations rather than the other, since neither is truly in conservative form. The physical interpretation of the conservative form of the equations for fluid dynamics has been discussed in the past.[9,13] If, for example,

the total flux of vorticity is conserved for a finite volume in the region of interest, then the vorticity transport equation is said to be in conservative form. Equations (3.21) and (3.23) have previously been referred to, by inspection, as conservative forms by several investigators. This misconception results from the natural transfer of vast experience with the planar equations to the much less frequently used axisymmetric equations. In other words, the identical procedure of adding a modified version of the continuity equation to the convection terms of the vorticity dynamic equation is used in both planar and axisymmetric cases. In both cases, this puts the convective terms into the conservative form without affecting the diffusion terms. In the planar case, this simple manipulation produces the conservative form desired. In the axisymmetric case, however, this is not true since the term $\frac{1}{r}\frac{\partial \omega}{\partial r}$ in the diffusion part is not in the proper form. This point has only recently been discussed[14] for curvilinear coordinate systems.

3.6 The Mean Field Equations to be Solved

In the light of this discussion the following form of the nondimensional system of equations will be considered in this study because they have been found to have the best conservation properties:

$$\frac{\partial}{\partial z}\left(\frac{1}{r}\frac{\partial \psi}{\partial z}\right) + \frac{\partial}{\partial r}\left(\frac{1}{r}\frac{\partial \psi}{\partial r}\right) + r\Omega = 0 \qquad (3.28)$$

$$\frac{\partial}{\partial z}(ru\Omega) + \frac{\partial \psi}{\partial r}(rv\Omega) = \frac{1}{r^2}\{\frac{\partial}{\partial z}[r^3 \frac{\partial}{\partial z}(\nu\Omega)] + \frac{\partial}{\partial r}[r^3 \frac{\partial}{\partial r}(\nu\Omega)] + S_\Omega\} \quad (3.29)$$

where the new variable Ω is defined to be

$$\Omega = \frac{\omega}{r}$$

and S_Ω is the source term of Ω defined to be created only from the turbulent variables:

$$S_\Omega = [(\frac{\partial u}{\partial r} + \frac{\partial v}{\partial z})(\frac{\partial^2 \nu}{\partial z^2} - \frac{\partial^2 \nu}{\partial r^2}) + 2(\frac{\partial v}{\partial r} - \frac{\partial u}{\partial z}) \frac{\partial^2 \nu}{\partial z \partial r} + (\frac{\partial \nu}{\partial z} \nabla^2 v - \frac{\partial \nu}{\partial r} \nabla^2 u) - \frac{2}{3} \frac{\partial^2}{\partial r \partial z}(kr)] \quad (3.30a)$$

and

$$\nu = \frac{1}{Re} + \nu_t \quad (3.30b)$$

$$\nu_t = C_\mu \frac{k^2}{\varepsilon} \quad (3.30c)$$

The equations for the turbulence model's quantities, k-ε, are given by eqs. (3.5)-(3.8). The conservative form of these equations is:

$$\frac{\partial}{\partial z}(ruk) + \frac{\partial}{\partial r}(rvk) = \frac{\partial}{\partial z}[r(\frac{\nu_t}{\sigma_k} + \frac{1}{Re}) \frac{\partial k}{\partial z}] + \frac{\partial}{\partial r}[r(\frac{\nu_t}{\sigma_k} + \frac{1}{Re}) \frac{\partial k}{\partial r}] + \nu_t G - \quad (3.31)$$

$$\frac{\partial}{\partial z}(ru\varepsilon) + \frac{\partial}{\partial r}(rv\varepsilon) = \frac{\partial}{\partial z}[r(\frac{\nu_t}{\sigma_\varepsilon} + \frac{1}{Re}) \frac{\partial \varepsilon}{\partial z}] + \frac{\partial}{\partial r}[r(\frac{\nu_t}{\sigma_\varepsilon} + \frac{1}{Re}) \frac{\partial \varepsilon}{\partial r}] + C_1 \nu_t \frac{\varepsilon}{k} G - C_2 \frac{\varepsilon^2}{k} \quad (3.32)$$

where G is the generation of turbulence given in (1.7) as follows:

$$G = \left(\frac{\partial u}{\partial r} + \frac{\partial v}{\partial z}\right)^2 + 4\left[\left(\frac{\partial v}{\partial r}\right)^2 + \left(\frac{v}{r}\right)^2 + \frac{v}{r}\frac{\partial v}{\partial r}\right]$$

$$= \left(2\frac{\partial v}{\partial z} - r\Omega\right)^2 + 4\left[\left(\frac{\partial v}{\partial r}\right)^2 + \left(\frac{v}{r}\right)^2 + \frac{v}{r}\frac{\partial v}{\partial r}\right] \qquad (3.33)$$

Suggested values for the various constants[2] are given in eq. (3.9).

The final forms of the temperature and the species transport equations are:

$$\frac{\partial}{\partial z}(ruT) + \frac{\partial}{\partial r}(rvT) = \frac{\partial}{\partial z}\left(r\lambda\frac{\partial T}{\partial z}\right) + \frac{\partial}{\partial r}\left(r\lambda\frac{\partial T}{\partial r}\right) + \frac{1}{ReE}G + S_T \qquad (3.34)$$

$$\frac{\partial}{\partial z}(ruc) + \frac{\partial}{\partial r}(rvc) = \frac{\partial}{\partial z}\left(rD\frac{\partial c}{\partial z}\right) + \frac{\partial}{\partial r}\left(rD\frac{\partial c}{\partial r}\right) \qquad (3.35)$$

where

$$\lambda = \frac{1}{RePr}(1 + R_d) + \frac{\nu_t}{Pr_t} \qquad (3.36)$$

$$D = \frac{1}{ReSc} + \frac{\nu_t}{Sc_t} \qquad (3.37)$$

$$S_T = -A\left[1 - \frac{1}{2}(2z - 1)^4\right](1-r) \qquad (3.38)$$

4. NUMERICAL PREDICTION OF THE FLOW FIELD

4.1 Finite Difference Approximations for the Derivatives

Suppose that the finite two dimensional or axisymmetric region is subdivided by two families of lines parallel to the two coordinates z,r. For any point $P = (z_p, r_p)$, eight neighboring nodes are considered; they are located on the horizontal and vertical lines around P, not necessarily equally spaced. The eight neighboring nodes are given compass abbreviations, as seen in Fig. 4.1. Thus, SE stands for the point $(z_p + h_E,\ r_p - h_S)$, etc. Let $\phi(NE)$, $\phi(P)$, etc. denote the values of $\phi(z,r)$ at the points NE, P, etc.

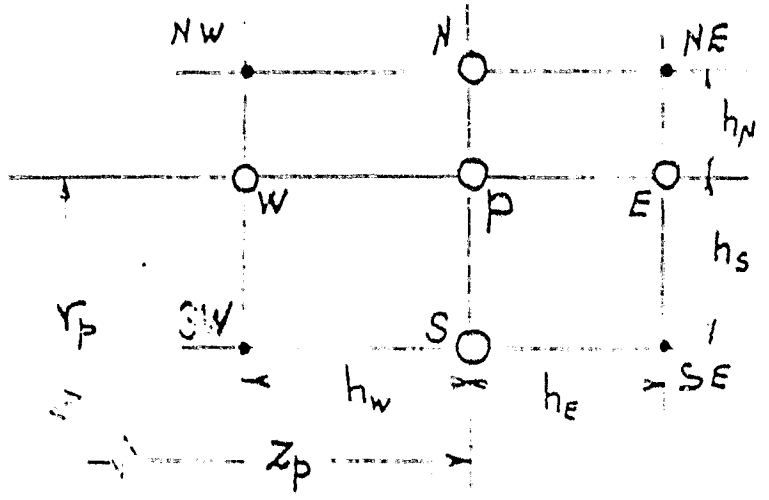

Fig. 4.1. Node Abbreviations for a Non-Constant Spaced Normal Grid Mesh.

An approximation to the first derivative ϕ_z at the point P can be obtained by considering the Taylor's series with a remainder in the two points E and W.

$$\phi_E = \phi_P + \phi_{z_p} h_E + \frac{1}{2} \phi_{zz_p} h_E^2 + \frac{1}{6} \phi_{zzz}(\zeta_E)\ h_E^3 \qquad (4.1)$$

$$z_p < \zeta_E < z_E$$

$$\phi_w = \phi_p - \phi_{z_p} h_w + \frac{1}{2} \phi_{zz_p} h_w^2 - \frac{1}{6} \phi_{zzz}(\zeta_w) h_w^3 \qquad (4.2)$$

$$z_w < \zeta_w < z_p$$

Solving (4.1) and (4.2) for ϕ_{z_p} eliminating ϕ_{zz_p} assuming that ϕ_{zzz} is continuous, one can get:

$$\phi_{z_p} = \frac{h_w}{h_E(h_E+h_w)} \phi_E + \frac{h_E-h_w}{h_E h_w} \phi_P - \frac{h_E}{h_w(h_E+h_w)} \phi_w + O(h^2) \qquad (4.3)$$

where $h = \max(h_w, h_E)$. Equation (4.3) has a truncation error OF the first z derivative $R^{(z)}$ of the order h^2 with the form of:

$$R_P^{(z)} = - \frac{h_E h_w}{6} \phi_{zzz}(\zeta) \qquad z_w \leq \zeta \leq z_E \qquad (4.4)$$

The analogous formula for ϕ_{r_p} is of similar form and obvious. This formulation is from the centered differences for ϕ_z, which is far better than that from the forward differences which can be obtained from eq. (4.1)

$$\phi_{z_p} = \frac{\phi_E - \phi_P}{h_E} \qquad (4.5)$$

or from the backward differences which can be obtained from eq. (4.2)

$$\phi_{z_p} = \frac{\phi_P - \phi_w}{h_w} \qquad (4.6)$$

These are only first order accurate.

The analogous second derivative may be obtained by similar Taylor expansions, like eqs. (4.1), (4.2) carrying one term further.

Solving for ϕ_{zzz_P} and eliminating the derivative ϕ_{z_P}, one can obtain the following expression:

$$\phi_{zzz_P} = \frac{2}{h_E(h_E+h_W)}\phi_E + \frac{2}{h_W(h_E+h_W)}\phi_W - \frac{1}{h_E h_W}\phi_P + R_P^{(zzz)} \qquad (4.7)$$

where the truncation error is:

$$R_P^{(zzz)} = -\frac{h_E-h_W}{3}\phi_{zzzz_P} + \frac{1}{12}(h_E^2 - h_E h_W + h_W^2)\phi_{zzzzz}(\xi) \qquad (4.8)$$

$$z_W < \xi < z_E$$

It is obvious that $R_P^{(zzz)}$ is not accurate to the second order. However, if the grid spacing is designed to be a smooth function of z, then $h_E - h_W = O(h^2)$ and the scheme is second order accurate. When $h_E = h_W$, eqs. (4.3) and (4.8) reduced to the known forms for a uniform grid:

$$\phi_{z_P} = \frac{\phi_E - \phi_W}{h_E+h_W} + O(h^2) \qquad (4.9)$$

$$\phi_{zz_P} = \frac{\phi_E - 2\phi_P + \phi_W}{\frac{1}{4}(h_E+h_W)^2} + O(h^2) \qquad (4.10)$$

One may argue that for a smooth grid spacing, eq. (4.3) may be reduced to eq. (4.9). Both approximations for ϕ_z on a nonuniform grid, (4.3) and (4.8) were tested (Roache[15]). Equation (4.3) was found to give a better approximation for ϕ_z, especially in the high gradient regions of the field.

4.2 Finite Difference Approximations to the Governing Equations

A quantitative description of the flow field under consideration is obtained by replacing the various derivatives in the governing equations with finite difference approximations and solving the algebraic system of equations. Before doing this the method of solving this system should be determined. It does not mean that a choice between a direct solution method or an iteration method has to be made first, but rather that the way of coupling the different variables of the field should first be considered since it will affect the form of the finite difference approximation. The finite difference models of the advection in the governing equations will be discussed first followed by the method of solution.

4.2.1 The Convective Terms

It is known that central difference approximations of the convective terms may give rise to instabilities.[35] These can be eliminated by employing one-sided difference schemes which assure that the flow numerical information is consistent with the physical flow. This improvement was introduced in 1953 and is discussed by some authors.[9,11,13] This idea was incorporated[16] in the definition of the "transportive property" which states, "A finite difference formulation of a flow equation possesses the transportive property if the effect of a perturbation in a transport property is advected only in the direction of the velocity." The finite-difference expressions of the convective terms which satisfy this property are called upwind

or upstream differences and depend upon the direction of the velocity component at each point. Two methods for carrying out this idea were formulated. In the first method, backward differencing for the advection terms is used if all the velocities in the neighborhood of a typical point P are positive, and forward differencing if all the velocities at this point are negative, that is:

$$\frac{\partial}{\partial x}(u\phi)^n = \begin{cases} [u_P^n \phi_P^n - u_W^n \phi_W^n]/h_W & \text{if} \quad u_P^n \geq 0 \\ [u_E^n \phi_E^n - u_P^n \phi_P^n]/h_E & \text{if} \quad u_P < 0 \end{cases} \tag{4.11}$$

$$\frac{\partial}{\partial y}(v\phi)^n = \begin{cases} [v_P^n \phi_P^n - v_S^n \phi_S^n]/h_S & \text{if} \quad v_P \geq 0 \\ [v_N^n \phi_N^n - v_P^n \phi_P^n]/h_N & \text{if} \quad v_P < 0 \end{cases} \tag{4.12}$$

A similar formulation may be obtained by using the control volume approach which provides a conservative and transportive differencing method to handle these equations. Unfortunately, the increase in stability gained by upstream differencing is at the cost of accuracy. The truncation error of the convective terms is increased to the first order, reducing the formal accuracy of the method to first order. Upstream differencing has gained popularity in spite of this criticism, and it has been found, from a practical point of view, to recover almost the same order of accuracy as central differencing. The upstream differencing was found[17] (by comparing about six different explicit methods)

to be the best compromise between accuracy and computing time. It was also found[18] that the upstream differencing of conservative forms yielded results which were as accurate as those from the second order difference equations.

Another upwind differencing method is known as the "donar cell" method. This technique[19] is similar to the above upwind technique, with the added advantage of retaining the property of second-order-like accuracy of centered space derivatives. However, it can be shown that in axisymmetric form the accuracy is still reduced to the first order. The K-R technique[20] for differencing the convective terms is known to be second-order accurate in the converging state, and unconditionally stable during the course of iterations. This is because it is an upwind differencing technique with a correction to recover the second order accuracy which is treated explicitly from the previous iteration (or time step). For example, the z convection of the quantity ϕ will be differenced as:

$$\frac{\partial}{\partial z}(u\phi)^n = \gamma_z \frac{u_E^n \phi_E^n - u_P^n \phi_P^n}{h_E} + (1-\gamma_z) \frac{u_P^n \phi_P^n - u_W^n \phi_W^n}{h_W}$$

$$+ (1 - \gamma_z - \gamma_z \frac{h_W}{h_E}) D_z^{n-1} \qquad (4.13)$$

where

$$D_z = \frac{1}{h_E+h_W} [u_E\phi_E + \frac{h_E}{h_W} u_W\phi_W - (\frac{h_E}{h_W} + 1) u_P\phi_P] \qquad (4.14)$$

and

$$\gamma_z = 0 \quad \text{if} \quad u_p \geq 0$$

$$\gamma_z = 1 \quad \text{if} \quad u_p < 0 \tag{4.15}$$

Similar expressions are used for $\frac{\partial}{\partial r}(v\phi)$, with a parameter γ_r instead of γ_z in eqs. (4.13)-(4.15). The upper indices n and n-1 refer to the appropriate time levels. In the steady state (convergence state) $\phi^n = \phi^{n+1}$, and eq. (4.13) represents a finite difference for the first derivative $\frac{\partial}{\partial z}(u\phi)$ of second order accuracy.

4.2.2 Modeling of Non-Linearities and Coupling

One of the main differences between the approach using the primitive variables and the approach using the vorticity-stream function variables to obtain numerical solutions of the two dimensional flow equations is in the treatment of the advection. In the primitive variables approach the convection is non-linear since products of the variables and their derivatives appear. In the regular ψ-ω (or ψ-Ω) approach the velocities appear only as coefficients of the vorticity derivatives and the ψ and ω variables appear in a sort of quasi-linear form.

As has been stated in many works[4,9] the ψ-ω solution method has to be under-relaxed in order for it to converge (also with upwind differencing) and this is due to the instabilities that the boundary condition for the vorticity introduce into the field. Since the boundary conditions for ω consist of linear relations between ψ and ω [see Section 4.3.2] it is reasonable to assume that the coupled solution of the two equations for ψ and ω will

result in suppression and possibly elimination of the instabilities. A simple way of coupling the ψ-ω equations is to leave their finite difference forms as in the separate case, where the coupling between ψ and ω is done only on the boundaries. A more intensive way of doing it is by coupling the ψ and ω variables at every point of the field.[21] In this case the following second order approximation for the nonlinearities of the convection in the non-conservation form is considered:

$$[u \frac{\partial}{\partial x} (\omega)]^n = u^{n-1} \frac{\partial}{\partial x} (\omega^n) + u^n \frac{\partial}{\partial x} (\omega^{n-1}) - u^{n-1} \frac{\partial}{\partial x} (\omega^{n-1}) \tag{4.16}$$

where n is again the time (or iteration) level. Applying the continuity equation (3.1) and the stream function definition (3.22), the following equation can be obtained for the planar vorticity convection.[9]

$$[u \frac{\partial \omega}{\partial x} + v \frac{\partial \omega}{\partial y}]^n = \underbrace{\frac{\partial}{\partial x} (u^{n-1} \omega^n)}_{\text{I}} + \underbrace{\frac{\partial}{\partial y} [\psi^n (\frac{\partial \omega}{\partial x})^{n-1}]}_{\text{II}} - \underbrace{\frac{\partial}{\partial x} (u^{n-1} \omega^{n-1})}_{\text{III}}$$

$$+ \underbrace{\frac{\partial}{\partial y} (v^{n-1} \omega^n)}_{\text{IV}} - \underbrace{\frac{\partial}{\partial x} [\psi^n (\frac{\partial \omega}{\partial y})^{n-1}]}_{\text{V}} - \underbrace{\frac{\partial}{\partial y} (v^{n-1} \omega^{n-1})}_{\text{VI}} \tag{4.17}$$

In the above equation, terms III and VI are source terms known explicitly from the previous time step. Terms I and IV represent the convection of the vorticity and may be treated by the K-R

method presented in eq. (4.13). Terms II and IV are new terms which represent the convection of the stream function in the vorticity equation. It can be easily shown that the diagonal dominance of the coupled system as well as the stability conditions will not be affected if the terms II and V will be central differenced or upwind differenced.

4.2.3 The Governing Equations

As was mentioned in section 3.6, the quantity Ω defined by

$$\Omega = \frac{\omega}{r}$$

has "better" conservation properties than the vorticity ω itself. The ψ-Ω relation is given in eq. (3.28) and the dynamic equation for Ω is given by eq. (3.2a), or by the following equation in the non-conservative form

$$u \frac{\partial \Omega}{\partial z} + v \frac{\partial \Omega}{\partial r} = \frac{\partial^2}{\partial z^2} (\mu\Omega) + \frac{\partial^2}{\partial r^2} (\mu\Omega) + \frac{3}{r} \frac{\partial}{\partial r} (\mu\Omega) + \frac{S_\Omega}{r} \qquad (4.18)$$

where $\mu = \mu_\ell + \mu_t$ is the total viscosity coefficient. Let us define the following grid parameters at the point P:

$$h_z = \frac{1}{2} (h_E + h_w), \qquad h_r = \frac{1}{2} (h_N + h_S),$$

$$\sigma_z = h_E / h_w, \qquad \sigma_r = h_N / h_S \qquad (4.19)$$

The finite difference form of the stream-function vorticity relation, eq. (3.28), will be

$$\psi_N \{\frac{1}{h_r^2} [\frac{1+\sigma_r}{\sigma_r^2} \frac{1}{1+\frac{r_N}{r_p}} + \frac{1}{2} (1 - \frac{1}{\sigma_r^2})]\}$$

$$+ \psi_S \{\frac{1}{h_r^2} [\sigma_r(1+\sigma_r) \frac{1}{1+\frac{r_S}{r_p}} - \frac{\sigma_r^2}{2} (1 - \frac{1}{\sigma_r^2})]\}$$

$$+ \psi_E \{\frac{1}{h_z^2} [\frac{1+\sigma_z}{2\sigma_z}]\}$$

$$+ \psi_W \{\frac{1}{h_z^2} [\frac{1+\sigma_z}{2}]\}$$

$$- \psi_P \{\frac{1}{h_r^2} [(1+\sigma_r)(\frac{1}{\sigma_r^2(1+\frac{r_N}{r_p})} + \frac{\sigma_r}{1+\frac{r_S}{r_p}}) - \frac{1}{2}(\sigma_r - \frac{1}{\sigma_r})^2] + \frac{1}{h_z^2} [\frac{(1+\sigma_z)^2}{2\sigma_z}]\}$$

$$+ \Omega_p \{r_p^2\} = 0 \qquad (4.20)$$

This equation is taken always to be at the new time level, say, n.

The finite difference form of the vorticity dynamic equation (3.29) will be:

$$\psi_N [\frac{1}{2h_r} \frac{A_N^{n-1}}{\sigma_r}]$$

$$+ \psi_S [- \frac{\sigma}{2h_r} A_S^{n-1}]$$

$$+ \psi_E [\frac{1}{2h_z} \frac{B_E^{n-1}}{\sigma_z}]$$

$$+ \psi_W [- \frac{\sigma_z}{2h_z} B_W^{n-1}]$$

$$+ \psi_P [\frac{1}{2h_r} (\sigma_r - \frac{1}{\sigma_r}) A_p^{n-1} + \frac{1}{2h_z} (\sigma_z - \frac{1}{\sigma_z}) B_p^{n-1}] +$$

$$+ \Omega_E \{-r_p \mu_E^{n-1} \frac{1+\sigma_z}{2\sigma_z} \frac{1}{h_z^2}\}$$

$$+ \Omega_w \{-r_p \mu_w^{n-1} \frac{1+\sigma_z}{2} \frac{1}{h_z^2}\}$$

$$+ \Omega_N \{-r_p \mu_N^{n-1} \frac{1+\sigma_r}{2\sigma_r} \frac{1}{h_r^2} - \frac{3}{2h_r} \mu_N^{n-1} \frac{1}{\sigma_r}\}$$

$$+ \Omega_S \{-r_p \mu_S^{n-1} \frac{1+\sigma_r}{2} \frac{1}{h_r^2} + \frac{3}{2h_r} \mu_s^{n-1} \sigma_r\}$$

$$+ \Omega_p \{r_p \mu_P^{n-1} [\frac{(1+\sigma_r)^2}{2\sigma_r} \frac{1}{h_r^2} + \frac{(1+\sigma_z)^2}{2\sigma_z} \frac{1}{h_z^2}] - \frac{3\mu_p^{n-1}}{2h_r} (\sigma_r - \frac{1}{\sigma_r})\}$$

$$+ \begin{cases} \text{if } u \geq 0 & \Omega_P(\frac{1+\sigma_z}{2h_z} r_P u_P^{n-1}) + \Omega_w(-\frac{1+\sigma_z}{2h_z} r_P u_w^{n-1}) + D_z^{n-1}(\Omega) \\ \text{if } u < 0 & \Omega_P(-\frac{1+\sigma_z}{2\sigma_z h_z} r_P u_P^{n-1}) + \Omega_E(-\frac{1+\sigma_z}{2\sigma_z h_z} r_P u_E^{n-1}) - \frac{D_z^{n-1}(\Omega)}{\sigma_z} \end{cases}$$

$$+ \begin{cases} \text{if } v \geq 0 & \Omega_P(\frac{1+\sigma_r}{2h_r} r_P v_P^{n-1}) + \Omega_S(-\frac{1+\sigma_r}{2h_r} r_S v_S^{n-1}) + D_r^{n-1}(\Omega) \\ \text{if } v < 0 & \Omega_P(-\frac{1+\sigma_r}{2\sigma_r h_r} r_P v_P^{n-1}) + \Omega_N(\frac{1+\sigma_r}{2\sigma_r h_r} r_N v_N^{n-1}) - \frac{D_r^{n-1}(\Omega)}{\sigma_r} \end{cases}$$

$$+ R^{n-1} = 0 \qquad (4.21)$$

where

$$A_N = \frac{1}{2h_z}\left[\frac{\Omega_{NE}}{\sigma_z} - \sigma_z\Omega_{NW} + \left(\sigma_z - \frac{1}{\sigma_z}\right)\Omega_N\right] \tag{4.22a}$$

$$A_S = \frac{1}{2h_z}\left[\frac{\Omega_{SE}}{\sigma_z} - \sigma_z\Omega_{SW} + \left(\sigma_z - \frac{1}{\sigma_z}\right)\Omega_S\right] \tag{4.22b}$$

$$A_P = \frac{1}{2h_z}\left[\frac{\Omega_E}{\sigma_z} - \sigma_z\Omega_w + \left(\sigma_z - \frac{1}{\sigma_z}\right)\Omega_p\right] \tag{4.22c}$$

$$B_E = \frac{1}{2h_r}\left[\frac{\Omega_{NE}}{\sigma_r} - \sigma_r\Omega_{SE} + \left(\sigma_r - \frac{1}{\sigma_r}\right)\Omega_E\right] \tag{4.22d}$$

$$B_w = \frac{1}{2h_r}\left[\frac{\Omega_{NW}}{\sigma_r} - \sigma_r\Omega_{SW} + \left(\sigma_r - \frac{1}{\sigma_r}\right)\Omega_w\right] \tag{4.22e}$$

$$B_p = \frac{1}{2h_r}\left[\frac{\Omega_N}{\sigma_r} - \sigma_r\Omega_S + \left(\sigma_r - \frac{1}{\sigma_r}\right)\Omega_P\right] \tag{4.22f}$$

$$D_z(\Omega) = \frac{r_p}{2h_z}\left[u_E\Omega_E - (1+\sigma_z)\,u_p\Omega_P + \sigma_z u_w\Omega_w\right] \tag{4.23a}$$

$$D_r(\Omega) = \frac{1}{2h_r}\left[r_N v_N\Omega_N - (1+\sigma_r)\,r_p v_p\Omega_P + \sigma_r r_s v_s\Omega_s\right] \tag{4.23b}$$

$$R = -\left\{\frac{r_p}{2h_z}\left[\frac{u_E\Omega_E}{\sigma_z} - \sigma_z\,u_w\Omega_w + \left(\sigma_z - \frac{1}{\sigma_z}\right)u_p\Omega_p\right]\right.$$

$$\left. + \frac{1}{2h_r}\left[\frac{r_N v_N\Omega_N}{\sigma_r} - \sigma_r r_s v_s\Omega_s + \left(\sigma_r - \frac{1}{\sigma_r}\right)r_p v_p\Omega_p\right]\right\} \tag{4.24}$$

This equation is solved at the n time level where all the coefficients u, μ and the source terms D_z, D_r and R are taken in the n-1 time level.

4.2.4 The k-ε Equations

The solution of the k-ε equations, (3.31-3.32), is obtained in this study in a coupled manner, based on a known flow field mean velocity distribution. The nonlinear terms are quasi-linearized with respect to the time level (or iteration index) n:

$$\left(\frac{\varepsilon}{k}\right)^n = \frac{\varepsilon^n}{k^{n-1}} + \frac{\varepsilon^{n-1}}{(k^2)^{n-1}} k^n - \frac{\varepsilon^{n-1}}{k^{n-1}} \tag{4.25a}$$

$$\frac{\varepsilon^2}{k} = \frac{2\varepsilon^{n-1}}{k^{n-1}} \varepsilon^n + \frac{(\varepsilon^2)^{n-1}}{(k^2)^{n-1}} k^n - 2\left(\frac{\varepsilon^2}{k}\right)^{n-1} \tag{4.25b}$$

$$\frac{k^2}{\varepsilon} = \frac{2k^{n-1}}{\varepsilon^{r-1}} k^n + \left(\frac{k^2}{\varepsilon^2}\right)^{n-1} \varepsilon^n - 2\left(\frac{k^2}{\varepsilon}\right)^{(n-1)} \tag{4.25c}$$

The finite difference approximation of the k equation (3.31) is:

$$k_E \left[-r_P \bar{\nu}_E^k \frac{1+\sigma_z}{2\sigma_z} \frac{1}{h_z^2}\right]$$

$$+ k_W \left[-r_P \bar{\nu}_W^k \frac{1+\sigma_z}{2} \frac{1}{h_z^2}\right]$$

$$+ k_N \left[-r_N \bar{\nu}_N^k \frac{1+\sigma_r}{2\sigma_r} \frac{1}{h_r^2}\right]$$

$$+ k_S \left[-r_S \bar{\nu}_S^k \frac{1+\sigma_r}{2} \frac{1}{h_r^2}\right]$$

$$+ k_P \left\{r_P \bar{\nu}_P^k \left[\frac{(1+\sigma_r)^2}{2\sigma_r} \frac{1}{h_r^2} + \frac{(1+\sigma_z)^2}{2\sigma_z} \frac{1}{h_z^2}\right] - 2C_\mu G \frac{k^{n-1}}{\varepsilon^{n-1}}\right\}$$

(continued)

$$+ \varepsilon_P \{-2C_\mu G_P (\frac{k^2}{\varepsilon^2})^{n-1} + 1\}$$

$$+ \begin{cases} \text{if } u \geq 0 & k_P(\frac{1+\sigma_z}{2h_z} r_P u_P^{n-1}) + k_w(-\frac{1+\sigma_z}{2h_z} r_P u_w^{n-1}) + D_z^{n-1}(k) \\ \text{if } u \leq 0 & k_P(-\frac{1+\sigma_z}{2\sigma_z h_z} r_P u_P^{n-1}) + k_E(\frac{1+\sigma_z}{2\sigma_z h_z} r_P u_E^{n-1}) - \frac{D_z^{n-1}(k)}{\sigma_z} \end{cases}$$

$$+ \begin{cases} \text{if } v \geq 0 & k_P(\frac{1+\sigma_r}{2h_r} r_P v_P^{n-1}) + k_s(-\frac{1+\sigma_r}{2h_r} r_s v_s^{n-1}) + D_r^{n-1}(k) \\ \text{if } v < 0 & k_P(-\frac{1+\sigma_r}{2\sigma_r h_r} r_P v_P^{n-1}) + k_N(\frac{1+\sigma_r}{2\sigma_r h_r} r_N v_N^{n-1}) - \frac{D_r^{n-1}(k)}{\sigma_r} \end{cases}$$

$$+ R_P^k = 0 \qquad (4.26)$$

and the finite difference approximation of the ε equation (3.32) is:

$$+ \varepsilon_E[-r_P \bar{\nu}_E \frac{1+\sigma_z}{2\sigma_z} \frac{1}{h_z^2}]$$

$$+ \varepsilon_w[-r_P \bar{\nu}_w^\varepsilon \frac{1+\sigma_z}{2} \frac{1}{h_z^2}]$$

$$+ \varepsilon_N[-r_N \bar{\nu}_N^\varepsilon \frac{1+\sigma_r}{2\sigma_r} \frac{1}{h_r^2}]$$

$$+ \varepsilon_S[-r_S \bar{\nu}_S^\varepsilon \frac{1+\sigma_r}{2} \frac{1}{h_r^2}]$$

$$+ \varepsilon_P \{r_P \bar{\nu}_P^\varepsilon [\frac{(1+\sigma_r)^2}{2\sigma_r h_r^2} + \frac{(1+\sigma_z)^2}{2\sigma_z h_z^2}] + 2C_2 (\frac{\varepsilon}{k})^{(n-1)}\}$$

(continued)

$$+ k_p \left[-C_1 C_\mu G_p + C_2 \left(\frac{\varepsilon}{k}\right)^{2(n-1)}\right]$$

$$+ \begin{cases} \text{if } u \geq 0 & \varepsilon_p \left(\frac{1+\sigma_z}{2h_z} r_p u_p^{n-1}\right) + \varepsilon_w \left(-\frac{1+\sigma_z}{2h_z} r_p u_w^{n-1}\right) + D_z^{n-1}(\varepsilon) \\ \text{if } u < 0 & \varepsilon_p \left(-\frac{1+\sigma_z}{2\sigma_z h_z} r_p u_p^{n-1}\right) + \varepsilon_E \left(\frac{1+\sigma_z}{2\sigma_z h_z} r_p u_E^{n-1}\right) - \frac{D_z^{n-1}(\varepsilon)}{\sigma_z} \end{cases}$$

$$+ \begin{cases} \text{if } v \geq 0 & \varepsilon_p \left(\frac{1+\sigma_r}{2h_r} r_p v_p^{n-1}\right) + \varepsilon_s \left(-\frac{1+\sigma_r}{2h_r} r_s v_s^{n-1}\right) + D_r^{n-1}(\varepsilon) \\ \text{if } v < 0 & \varepsilon_p \left(-\frac{1+\sigma_r}{2\sigma_r h_r} r_p v_p^{n-1}\right) + \varepsilon_N \left(\frac{1+\sigma_r}{2\sigma_r h_r} r_N v_N^{n-1}\right) - \frac{D_r^{n-1}(\varepsilon)}{\sigma_r} \end{cases}$$

$$+ R_p^\varepsilon = 0 \qquad (4.27)$$

where:

$$\bar{\nu}^k = \left(\mu_\ell + \frac{\mu_t}{\sigma_k}\right)/\rho \qquad (4.28a)$$

$$\bar{\nu}^\varepsilon = \left(\mu_\ell + \frac{\mu_t}{\sigma_\varepsilon}\right)/\rho \qquad (4.28b)$$

$$R_p^k = -2C_\mu G_p \left(\frac{\varepsilon^2}{k}\right)^{(n-1)} \qquad (4.29a)$$

$$R_p^\varepsilon = 2C_2 \left(\frac{k^2}{\varepsilon}\right)^{(n-1)} \qquad (4.29b)$$

The operators D_z and D_r are defined in eqs. (4.23), and the generation term, G, is defined in eq. (3.33), taking the velocities from the last time level, n-1.

The finite difference approximations for the temperature and species equations (3.35-3.36) may be obtained in a manner similar to that used for the above equations. The equations are linear and may be solved in an uncoupled manner.

4.3 The Boundary Conditions

The system of equations governing the flow field, (3.28-3.38), are of an elliptic nature and therefore boundary conditions for all the variables should be specified on all the boundaries. Four boundaries confine the present field: the outer cylinder wall, the axis of symmetry and the inlet and outlet cross-sectional planes. Although the main purpose of this study is to solve the turbulent flow, the program was checked with some laminar test cases and therefore the laminar boundary conditions will be also mentioned. Let us begin with the symmetry axis conditions.

4.3.1 The Axis of Symmetry

Along the symmetry axis the stream function has a constant value and it is convenient to choose it as zero:

$$\psi(r = 0) = 0 \tag{4.30}$$

so that ψ simulates the mass flux contained between r and 0. The values of Ω can be obtained from its dynamic equation (3.29) assuming symmetry, i.e.:

$$v = 0 \tag{4.31}$$

on this line. Therefore in the limit as $r \to 0$ that equation will assume the following form:

$$u \frac{\partial \Omega}{\partial z} = \frac{\partial^2}{\partial z^2} (\nu\Omega) + 4 \frac{\partial^2}{\partial r^2} (\nu\Omega) \tag{4.32}$$

with the restriction:

$$\frac{\partial \Omega}{\partial r} = \frac{\partial \nu}{\partial r} = 0 \tag{4.33}$$

at $r = 0$.

It is important to note that other formulae[4] for $\Omega(r=0)$ can be obtained by assuming above eq. (4.33) that the z derivatives in eq. (4.32) are negligible, and therefore with $\frac{\partial \Omega}{\partial r} = 0$ we can get that

$$\Omega(r = 0) = \text{const} = C \tag{4.34}$$

where the value of C can be evaluated from the ψ-Ω equation (3.28) with

$$\frac{\partial \psi}{\partial r} (r = 0) = 0 \tag{4.35}$$

since the limit for the centerline u velocity definition

$$u = \lim_{r \to 0} \frac{1}{r} \frac{\partial \psi}{\partial r} = \frac{\partial^2 \psi}{\partial r^2}\bigg|_{r=0} \tag{4.36}$$

exists. In the present approach, both equations for ψ and Ω are solved exactly on the axis of symmetry. Since

$$\frac{\partial T}{\partial r} = \frac{\partial C}{\partial r} = \frac{\partial k}{\partial r} = \frac{\partial \varepsilon}{\partial r} = 0 \tag{4.37}$$

on the axis of symmetry the dynamic equations for k, ε, T and C on this line may be derived from equations (3.31), (3.32), (3.34), (3.35) giving the following set:

$$\frac{\partial}{\partial z}(uk) = \frac{\partial}{\partial z}\left[\left(\frac{\nu_t}{\sigma_k} + \frac{1}{Re}\right)\frac{\partial k}{\partial z}\right] + \left(\frac{\nu_t}{\sigma_k} + \frac{1}{Re}\right)\frac{\partial^2 k}{\partial r^2} + \nu_t G - \varepsilon \qquad (4.38a)$$

$$\frac{\partial}{\partial z}(u\varepsilon) = \frac{\partial}{\partial z}\left[\left(\frac{\nu_t}{\sigma_\varepsilon} + \frac{1}{Re}\right)\frac{\partial \varepsilon}{\partial z}\right] + \left(\frac{\nu_t}{\sigma_\varepsilon} + \frac{1}{Re}\right)\frac{\partial^2 \varepsilon}{\partial r^2} + \frac{\varepsilon}{k}\left(C_1 \nu_t G - C_2 \varepsilon\right) \qquad (4.38b)$$

$$\frac{\partial}{\partial z}(uT) = \frac{\partial}{\partial z}\left(\lambda \frac{\partial T}{\partial z}\right) + \lambda \frac{\partial^2 T}{\partial r^2} + \frac{1}{ReE} G + S_T \qquad (4.38c)$$

$$\frac{\partial}{\partial z}(uc) = \frac{\partial}{\partial z}\left(D \frac{\partial c}{\partial z}\right) + D \frac{\partial^2 c}{\partial z^2} \qquad (4.38d)$$

$$G = 6\left(\frac{\partial u}{\partial z}\right)^2 \qquad (4.38e)$$

4.3.2 Solid Wall - Laminar Case

The stream function is constant on the wall since the mass flux of the flow does not change during its passage through the system. Concerning the laminar vorticity on the walls, with the classic approach the dynamic equation for Ω is not solved on the rigid wall surface, but rather the values of Ω_w are taken from the ψ-Ω relation (3.28). By using the no-slip conditions, $\left(\frac{\partial \psi}{\partial z}\right)_w = \left(\frac{\partial \psi}{\partial r}\right)_w = 0$, the following second order accurate values for Ω_w may be obtained by expanding ψ and Ω in a Taylor series about the wall point w:[22]

$$\Omega_w + \frac{r_1}{r_w}\,\frac{r_w + 3r_1}{3r_w + 5r_1}\,\Omega_1 = \frac{3(\psi_w - \psi_1)}{h^2 r_w^2\,(1 - \frac{5}{8}\,\frac{h}{r_w})} \tag{4.39}$$

for $r = r_w = \text{const}$ as shown in Fig. 4.2,

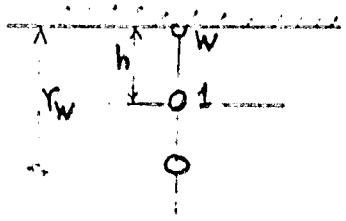

Fig. 4.2: Grid Near a Cylindrical Wall

and, for z = const as shown in Fig. 4.3:

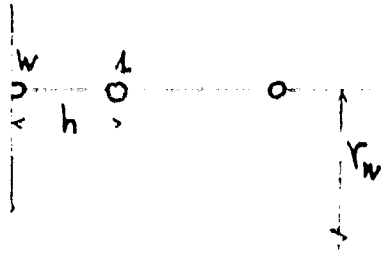

Fig. 4.3: Grid Near a Vertical Wall

$$\Omega_w + \frac{1}{2}\,\Omega_1 = \frac{3(\psi_w - \psi_1)}{h^2\, r_w^2} \tag{4.40}$$

where 1 is one point away from the wall point, w, into the field and h is the distance between the points 1 and w.

A different approach to get Ω_w on a r = const. = r_w wall is to impose the no slip condition (4.39) in the ψ-Ω relations to get

$$\Omega_w = -\frac{1}{r_w^2}\left(\frac{\partial^2\psi}{\partial r^2}\right)_w$$

with

$$\left(\frac{\partial\psi}{\partial r}\right)_w = 0$$

which gives:

$$\Omega_w = \frac{2}{r_w^2 h^2}(\psi_1 - \psi_w) + O(h^2) \qquad (4.41)$$

For a z = const. wall one can use the no slip condition to get

$$\left(\frac{\partial\psi}{\partial z}\right)_w = 0$$

And since ψ is constant along this wall an equation the same as (4.41) holds true.

4.3.3 Solid Wall - Turbulent Case

The main difficulty in imposing the turbulent boundary conditions on an impermeable wall is the matching between the turbulence model and the boundary condition formulation. Let us first discuss generally the nature of turbulence near a wall.

The above recommended k-ε model was developed based on certain assumptions concerning isotropy of ε and the relations between the Reynolds stress and the turbulent kinetic energy k, among

other assumptions. Those assumptions are not valid near a wall which has the following contradictory features:

(i) sharp flow properties variation.

(ii) the turbulent viscosity begins to affect the various turbulent processes due to the low turbulent energy level (or low turbulent Reynolds numbers).

(iii) the presence of the wall destroys any isotropy feature that is carried to it from the main stream.

There are two commonly employed ways of accounting for the turbulent phenomena in the wall region: (i) the wall function method and (ii) the method of modelling low turbulent Reynolds number phenomena. It is very common to divide the turbulent boundary layer with thickness δ, into two main parts: the inner layer, $0 \leq \frac{y}{\delta} \leq 0.2$, and the outer layer, $0.2 \leq \frac{y}{\delta} \leq 1.0$. The inner layer is dominated by the wall effects and the outer layer by the flow effects. Since the k-ε model was designed to account for the outer layer properties, the inner layer determines the turbulent boundary conditions. The influence of the inner layer depends on the relative size of the terms on the right hand side of the wall shear stress

$$\tau_w = \mu \frac{\partial U}{\partial y} - \rho \overline{u'v'} \tag{4.42}$$

where u', v' are the turbulent fluctuations in the longitudinal and lateral directions, and $-\rho \overline{u'v'}$ is the non-negligible Reynolds stress in the boundary layer. It is very convenient to

use the U^+ and y^+ formulation in the inner layer as follows:

$$U^+ = \frac{U}{v^*} \; ; \quad y^+ = \frac{y\, v^*}{\nu} \tag{4.43a,b}$$

where v^* is the shear velocity defined as

$$v^* = \sqrt{\tau_w/\rho} \tag{4.43c}$$

Three regions may be distinguished in the inner layer:

(i) The laminar sublayer: $0 < y^+ < 5$. This is the innermost part where

$$-\overline{u'v'} << \mu \frac{\partial U}{\partial y} \; , \quad \text{and} \tag{4.44a}$$

$$U^+ = y^+ \; ; \tag{4.44b}$$

(ii) The logarithmic law region: $40 < y^+ < 0.2\delta^+$. This is the outermost part where the only contribution to the stress is $-\rho\, \overline{u'v'}$, and

$$U^+ = \frac{1}{\kappa} \ell n\, y^+ + C \; , \qquad \kappa = 0.41 \quad \text{and} \quad C \approx 5.1$$

$$= \frac{1}{\kappa} \ell n\, (Ey^+) \; , \qquad E \approx 9.025 \tag{4.45}$$

(iii) The buffer region: $5 < y^+ < 40$. This is the intermediate part between the sublayer region and the logarithmic region.

In the "wall function" approach, the first grid point is located away from the wall, and the goal is to locate it in the logarithmic region. In this region τ_w and k^+ are constants, and

the generation balances the dissipation in the k equation (3.31):

$$v^* = C_\mu^{1/4}\, k^{1/2} \tag{4.46a}$$

$$\varepsilon = \frac{C_\mu^{3/4}\, k^{3/2}}{\kappa\, y} \tag{4.46b}$$

$$\mu_t = C_\mu^{1/4}\, \sqrt{k}\, \kappa\, y$$

where y is measured from the wall, and κ is the Von-Karman coefficient ($\simeq 0.41$).

From the balance between the ε generation and dissipation in eq. (3.32) one can get:

$$C_2 - C_1 = \frac{\kappa^2}{\sigma_\varepsilon\, C_\mu^{1/2}} \quad (\text{for } y^+ >> 1) \tag{4.47}$$

This equation is the only condition which assures that the k-ε model also holds in the logarithmic zone. Generally C_1 and C_2 as well as C_μ are constants found from the experimental data of one-dimensional turbulent grid flows.[2] It can be seen that the constants appearing in eq. (3.9) do not fulfill eq. (4.47).
In [7] another set is recommended:

$$C_\mu = 1\ ;\quad C_1 = 1.47\ ;\quad C_2 = 0.18\ ;\quad \sigma_k = 1\ ;\quad \sigma_\varepsilon = 1.3 \tag{4.48}$$

This set of constants is not in agreement with the one that was suggested for obtaining a good approximation to ε in the main stream field. Analyzing the turbulent quantities in the sublayer region, one might conclude that

$$k^+ \sim (y^+)^2\ ,\qquad \varepsilon^+ = \text{constant}\ . \tag{4.49}$$

Eqs. (4.49) leads to the following relationship between the model coefficients

$$(2C_1/C_\mu C_2) = y^4 \tag{4.50}$$

Therefore some papers[1,23] suggest a dependence of the model coefficients on the local turbulent Reynolds number R_t defined by

$$R_t = \frac{\varepsilon}{C_\mu k^2} \tag{4.51}$$

or on the y^+ normal distance. Such a variation can be obtained by adjusting the constants using some experimental data:[1]

$$C_2 = C_{2\infty} \left[1 - 0.3 \exp(-0.125 \cdot y^{+4})\right] \tag{4.52a}$$

$$C_\mu = C_{\mu\infty} \exp\left[-\frac{125}{50 + R_t}\right] \tag{4.52b}$$

It can be seen that these variations doe not resolve the above conflict since in the logarithmic zone the Reynolds number is highly turbulent. The above functions do allow us to locate the first grid point in the sublayer region, however.

The following set of constants was adopted in the present study to get good agreement with the axisymmetric experimental results:

$$C_1 = 1.5 \; ; \quad C_{2\infty} = 2.0 \; ; \quad C_{\mu\infty} = 0.09 \; ; \quad \sigma_\varepsilon = 1.12 \tag{4.53}$$

With the "wall function" approach the first grid point is not located on the wall but at a distance y away from the wall, as is illustrated in Fig. 4.4.

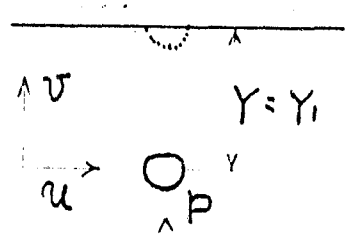

Fig. 4.4: Grid Near the Wall for a Turbulent Flow.

For this point p, located in the logarithmic region where y_o^+ is the sublayer edge, the following relations exist:

$$y^+ = y \frac{v^*}{\nu} \; ; \quad u^+ = \frac{u}{v^*} \; ; \quad u^+ = \frac{1}{K} \ln(E\, y^+) \qquad (4.54a,b,c)$$

$$\psi^+ = \frac{1}{2} y_o^+ - \frac{1}{K} y_o^+ [\ln(E\, y_o^+) - 1] - \frac{y_o^+}{K} [\ln(E\, y^+) - 1]$$

$$\approx y^+ (u^+ - 2.5) - 38.5 \qquad (4.54d)$$

$$\omega^+ = - \frac{1}{K y^+} = - \frac{2.5}{y^+} \qquad (4.54e)$$

$$K^+ = K_o^+ = 3.15 \qquad (4.54f)$$

$$\varepsilon^+ = \frac{C_\mu^{3/4}\, k^{+3/2}}{K} \frac{1}{y^+} = \frac{2.24}{y^+} \qquad (4.54g)$$

$$E = 9.0 \qquad (4.54h)$$

If the first grid point happens to be in the viscous sublayer, then:

$$u^+ = y^+ \; ; \quad \omega^+ = - 1 \; ; \quad \psi^+ = \frac{1}{2} y^{+2} \qquad (4.55a,b,c)$$

$$K^+ = 0.1\, y^{+2} \; ; \quad \varepsilon^+ = 0.2 \qquad (4.55d,e)$$

If the first grid point cannot be kept in the sublayer or logarithmic regions during the iterations, the approach of continuous wall functions can be adopted. In this case the first grid point may be located on the wall and the following boundary conditions have to be considered for the first grid point away from the wall:

$$\psi^+ = \frac{1}{2} y^+ u^+ + (1 - e^{-\alpha R_t})[\frac{1}{2} y^+(u^+ - 5) - 38.5] \tag{4.56a}$$

$$\omega^+ = -[1 + (1 - e^{-\alpha R_t})(\frac{2.5}{y^+} - 1)] \tag{4.56b}$$

$$k^+ = 0.1\, y^{+2} + (1 - e^{-\alpha R_t})(3.15 - 0.1\, y^{+2}) \tag{4.56c}$$

$$\varepsilon^+ = 0.2 + (1 - e^{-\alpha R_t})(\frac{2.25}{y^+} - 0.2) \tag{4.56d}$$

where

$$\alpha = 2.5 \tag{4.56e}$$

was chosen to match the experimental u^+ profiles.

In recent years[24] some carefully measurements of scalar quantities in the wall region have been carried out. The profiles of S^+ in the logarithmic region was found to satisfy the correlation

$$S^+ = \frac{1}{K_S} \ln y^+ + F \tag{4.57a}$$

with

$$K_S = 0.46$$

where S^+ is the dimensionless scalar (temperature or species) defined to be

$$S^+ = \frac{S_w - S}{\sqrt{D(\frac{\partial S}{\partial y})_w}} \tag{4.57b}$$

For the case of the species S = C, the boundary condition is

$$\left(\frac{\partial C}{\partial y}\right)_w = 0 \tag{4.58a}$$

and the Schmidt number is taken to be

$$Sc_t = \frac{K}{K_c} = 0.885 \tag{4.8b}$$

The turbulent Prandtl number was found to vary through the boundary layer region. The first suggestion[25] which was based on some measurements[26,27] was:

$$Pr_t = 0.9 - 0.4 \left(\frac{Y}{\delta}\right)^2 \tag{4.59a}$$

and was updated later[28] to

$$Pr_t = 0.95 - 0.45 \left(\frac{Y}{\delta}\right)^2 \tag{4.59b}$$

Since the adiabatic wall is not of interest in this study, the following temperature continuous wall function will be adopted:

$$\frac{T_w - T}{\sqrt{\lambda}\left(\frac{T}{Y}\right)_w} = y^+ + (1 - e^{-\alpha R_t})[2.15\ \ell n(12\ y^+) - y^+] \tag{4.60a}$$

$$Pr_t = 0.95 - 0.4 \left(\frac{Y}{\delta}\right)^2 \tag{4.60b}$$

and for the species equations (4.58a,b).

4.3.4 Inlet Conditions

In most problems the flow velocity temperature and the various concentrations are known in the inlet section i. Usually a fully developed U_i velocity profile is given from which ψ and Ω may be deduced:

$$\psi = \int_0^r y\, u_i(y)\, dy \tag{4.61a}$$

$$\Omega = \frac{1}{r}\frac{\partial u_i}{\partial r} \tag{4.61b}$$

For the laminar case u_i is taken as

$$u_i(r) = U_o\,(1 - \frac{r^2}{R^2}) \tag{4.62a}$$

and for the turbulent case the velocity defect law is adopted:

for highly turbulent Reynolds numbers:

$$U_o^+ - u^+ = (\frac{1}{K}\,\ell n\,\frac{R^+}{y^+})(1 - e^{-\alpha R_t}) + y^+\, e^{-\alpha R_t} \tag{4.62b}$$

for low turbulent Reynolds numbers:

$$\frac{u^+}{U_o^+} = (y^+)^{1/7} \tag{4.62c}$$

For the turbulent energy and the turbulent dissipation, we assume that we have the profiles that are described in equations (4.56c,d).

In order to have a close form of the system at the inlet, we have to specify the ratio

$$\beta = \frac{v^*}{U_o} \tag{4.63}$$

For laminar flow it can be shown that

$$\beta = \sqrt{\frac{2}{Re}} \tag{4.64}$$

and we shall assume similar β for the turbulent flow. In any event the inlet conditions have very little effect on the inner field solution, especially if the inlet section is taken to be far from the regions of high gradients.

4.3.5 Exit Conditions

At the outlet boundary we assume that the longitudinal diffusion is negligible, that is

$$\frac{\partial^2}{\partial z^2} \left\{ \begin{matrix} \text{all the} \\ \text{variables} \end{matrix} \right\} = 0 \tag{4.65}$$

and the flow is basically parabolic near the exit section.

4.3.6 Inner Tube Trailing Edge Conditions

The inner cylinder is indicated by the point p in Fig. 4.5.

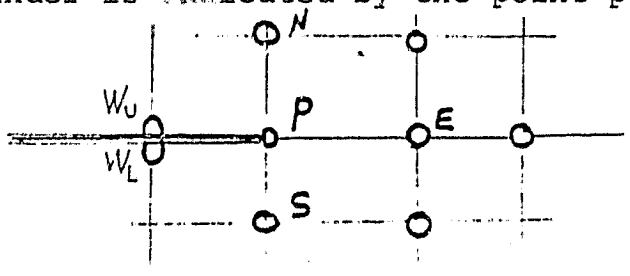

Fig. 4.5: End Wall Computational Region.

One approach[4] that is easy to use and most common to consider that the dividing stream line, ψ_p, has no curvature between point p and point E, satisfying, at the end wall,

$$\psi_E = \psi_p$$

The approach that will be used in this study is based on the physical fact that Ω has two different values at the point p, depending on whether the $\frac{\partial u}{\partial r}$ derivative is calculated from values above the wall (to give Ω_p^u) or from points below the wall (to give Ω_p^L). Those two values are opposite in sign. Solving the Ω equation at the point N, Ω_p^u will be used. Solving at the point S, the Ω_p^L will be used. When solving the equation at the point E, $\Omega_p = 0$ will be used since ψ_p is a separation line.

5. METHOD OF SOLUTION

The solution to the set of six finite difference equations is obtained in this study in an iterative manner since it is impossible to invert the entire system directly. We use the term, one global iteration of the flow field, here to mean that the following two piece chain is completed:

(i) For a given k-ε field the mean field quantities, i.e. ψ-Ω, are obtained to a certain convergence tolerance, including the velocity fields.

(ii) For these velocity fields the k-ε turbulent variables are obtained iteratively to a certain tolerance.

After the global iteration set converges, it is possible to solve the concentration field, C, and after convergence of this field it is possible to solve the temperature field. This iteration process may be sketched as follows:

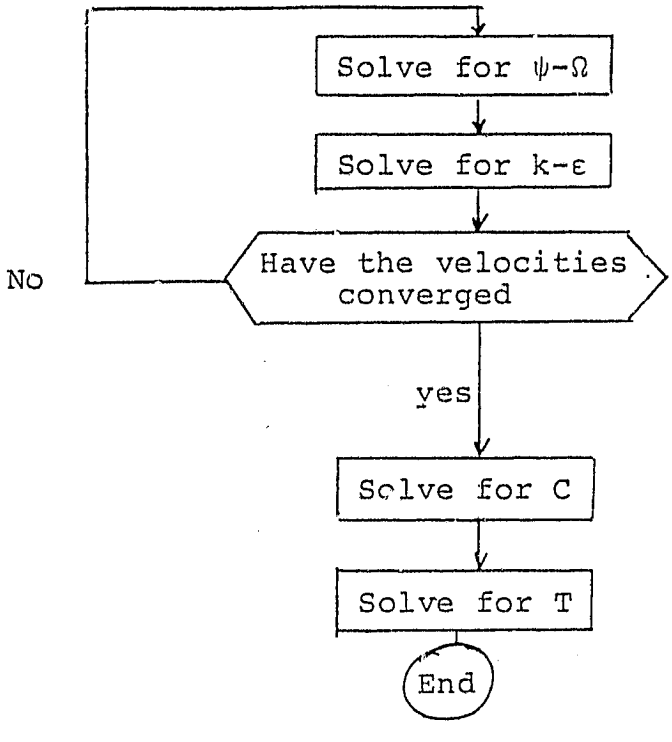

5.1 Solution Technique

The solutions of the scalar fields C and T are obtained by the successive line relaxation (SLR) technique. With this technique the scalar variable is solved implicitly for all the rows and then for all the columns in the field, replacing successively the old values by the current new values. The solution of the coupled systems, like ψ-Ω and k-ε, are obtained by the successive block line relaxation (SBLR), which is the same as the SLR technique but expressed in terms of blocks instead of scalars.

5.2 Stability Analysis

The basic blocked system that is solved here may be described by the following equation

$$[E]\ \underset{\sim}{\phi}_E + [w]\ \underset{\sim}{\phi}_W + [N]\ \underset{\sim}{\phi}_N + [S]\ \underset{\sim}{\phi}_S + [P]\ \underset{\sim}{\phi}_P + \underset{\sim}{R} = 0, \qquad (5.1)$$

where [E], [w], [N], [S] and [P] are the coefficient matrices (in the present study 2 x 2), $\underset{\sim}{R}$ is the source term vector and ϕ is the variable vector. The SBLR along the field columns may be written as

$$E^{n-1}\ \phi_E^{n-1} + w^{n-1}\ \phi_w^n + N^{n-1}\ \phi_N^n + S^{n-1}\ \phi_S^n + P_1^{n-1}\ \phi_P^n + (R^{n-1} + P_2^{n-1}\ \phi_P^{n-1}) = 0 \qquad (5.2)$$

where it is understood that E is a matrix and P is a vector.

The coefficient matrix [P] of the middle point is split into two matrices

$$[P] = [P_1] + [P_2]$$

where $[P_1]$ contains the total diffusion effect and the convection in the implicit direction [which is r in eq. (5.2)] and $[P_2]$ contains the effect of the convection in the other direction. Treating the $[P_1]$ contribution implicitly and the $[P_2]$ contribution explicitly has been found to be the best way of splitting of [P] for turbulent flow. For laminar flow, it is found to be best to set $[P_2] = 0$. This is due to the special boundary condition near the wall used with turbulent flows. The stability requirement is expressed in the diagonal dominance inequality:

$$|P_1| \geq \begin{cases} |w| + |E| \\ \text{and} \\ |S| + |N| \end{cases} \tag{5.3}$$

where strict inequality has to be maintained at least in one point of the field.

5.2.1 Stability of the ψ-Ω System

Let us check first the stability in the z-direction of the ψ-Ω system, eq. (4.20-4.21):

$$|E| + |w| = \frac{r_p(1+\sigma_z)^2}{4\, h_z^4 \sigma_z} \cdot \begin{cases} \nu_E \frac{1}{\sigma_z} + \nu_w + u_w h_z & \text{if } u \geq 0 \\ \frac{\nu_E}{\sigma_z} + \nu_w + \frac{|u_E| h_z}{\sigma_z} & \text{if } u < 0 \end{cases}$$

$$|P_2| = \Bigg| \left[\frac{1+\sigma_r}{h_r^2}\left(\frac{1}{\sigma_r^2(1+\frac{r_N}{r_p})} + \frac{\sigma_r}{1+\frac{r_s}{r_p}}\right) + \frac{(1+\sigma_z)^2}{2\sigma_z h_z^2} - \frac{1}{2h_r^2}\left(\sigma_r - \frac{1}{\sigma_r}\right)^2\right]$$

$$\left\{\frac{V_p r_p}{2}\left[\frac{(1+\sigma_r)^2}{\sigma_r}\frac{1}{h_r^2} + \frac{(1+\sigma_z)^2}{\sigma_z}\frac{1}{h_z^2} - \frac{3}{2h_r r_p}\left(\sigma_r - \frac{1}{\sigma_r}\right)\right]\right.$$

$$+ \frac{1+\sigma_z}{2h_z} r_p \cdot \begin{cases} u_p & \text{if } u > 0 \\ |u_p|/\sigma_z & \text{if } u < 0 \end{cases}$$

$$\left. + \frac{r_p^2}{2}\left[\frac{A_p}{h_r}\left(\sigma_r - \frac{1}{\sigma_r}\right) + \frac{B_p}{h_z}\left(\sigma_z - \frac{1}{\sigma_z}\right)\right]\right| \Bigg|$$

so that stability requires:

$$\left[\begin{cases} \text{if } u \geq 0 & + u_w h_z \\ \text{if } u < 0 & + \frac{|u_E|}{\sigma_z} h_z \end{cases} \right] \leq \left[\begin{array}{l} 2\,\frac{1+\sigma_r}{1+\sigma_z}\left(\frac{h_z}{h_r}\right)^2\left[\frac{1}{\sigma_r^2(1+\frac{r_N}{r_p})} + \frac{\sigma_r}{1+\frac{r_s}{r_p}}\right]|u_p| \\ \quad + \begin{cases} u_p h_z & \text{if } u \geq 0 \\ |u_p| h_z/\sigma_z & \text{if } u < 0 \end{cases} \\ \quad + 4(1+\sigma_r)\left(\frac{h_z}{h_r}\right)^2\left[\frac{1+\sigma_r}{2\sigma_r} + \frac{1}{\sigma_r^2(1+\frac{r_N}{r_p})}\right. \\ \quad \left. + \frac{\sigma_r}{1+\frac{r_s}{r_p}}\right]\nu_p + \left(\frac{1}{\sigma_z}+1\right)\nu_p \end{array}\right]$$

$$+ \frac{\nu_E}{\sigma_z} + \nu_w$$

(5.4)

It is reasonable to assume that σ_r and σ_z are analytic functions of r and z such that $\sigma - \frac{1}{\sigma} = O(h^2)$ and therefore may be neglected in the stability analysis. It can be seen from eq. (5.4) that this scheme is unconditionally stable and it is more stable than in the case where ψ and Ω are solved separately.[9] It can be shown, also, by checking the spectral radius of the ψ-Ω system, that the rate of convergence of the coupled system R_C is greater than that of the separate system R_S:*

$$\frac{R_C}{R_S} \approx 1 + \frac{1}{\frac{\sigma_z(1+\sigma_r)}{\sigma_r(1+\sigma_z)} \left(\frac{1}{\sigma_r^2} + 2\sigma_r\right) (Re_C + D)} + (h^2) \qquad (5.5)$$

where Re_C is the averaged cell Reynolds number

$$Re_C = (u_P h_z + v_P h_r) Re \qquad (5.6)$$

D is a positive function of the Ω derivatives $\frac{\partial \Omega}{\partial z}$ and $\frac{\partial \Omega}{\partial r}$, and is $O(h^2)$. Therefore, it may be concluded that the main improvement in the rate of convergence (and also in stability) of the coupled system results from treating the Ω in the ψ-Ω relations as an unknown rather than as a source term.

---

* R_S was taken to be the rate of convergence in the case that for every ψ solution, an Ω solution is obtained. In that case it may be proved that $R_S^2 \approx R_\psi \cdot R_\Omega$ where R_ψ and R_Ω are the rate of convergence of the ψ equation and of the Ω equation respectively.

Treating the convection by splitting it between ψ and Ω and in eq. (4.17) has second order (h^2) effects on the rate of convergence. But since it is hard to evaluate the coefficient of this effect, this split is used to obtain the results of this effect. No extensive study of this effect has been done but by using this technique a higher rate of convergence can be achieved. Generally, computer results have shown that the actual rate of convergence is higher than is predicted by eq. (5.5), since the boundary conditions are based only on the ψ-Ω relations.

5.2.2 Stability of the k-ε System

The stability condition for the k-ε system can be derived in a manner similar to that of the ψ-Ω system. It turns out that the upstream influence makes the system more stable. We consider first the zero velocity case. In this case the matrices E and W are positive definate, and therefore if P_1 is also positive definate we have:

$$\frac{r_p^2}{4h_z^4}(1+\sigma_z)^2\left[\frac{\bar{v}_E^k\,\bar{v}_W^\varepsilon}{\sigma_z^2}+\bar{v}_W^k\,\bar{v}_W^\varepsilon-\bar{v}_p^k\,\bar{v}_p^\varepsilon\,\frac{(1+\sigma_z)^2}{2\sigma_z}\right]$$

$$\geq \frac{r_p(1+\sigma_z)^2}{\sigma_z h_z^2}\left[\bar{v}_p^k\,C_2\,\frac{\varepsilon}{k}-C_\mu G\,\frac{k}{\varepsilon}\,\bar{v}_p\right]+C_2\,\frac{\varepsilon^2}{k^2}-2C_\mu^2\,C_1 G\,\frac{k^2}{\varepsilon}$$

$$-C_\mu(4C_2-C_1)\,G \qquad (5.7)$$

It may result that the possible critical points in the field for which this conditions should be checked, are the points in the logarithmic zone. Substituting the logarithmic relations, taking

into account only the leading terms (of y^+ powers), the following equations can be derived in terms of the "+" system, with $\sigma_r = \sigma_z = 1$

$$\frac{R}{h_z} > 4 \frac{C_\mu^{3/4} k^{+1/2}}{\kappa} \approx 2.85 \qquad (5.8)$$

where R is the outer cylinder radius and h_z is the distance of the second point away from the wall. This condition always holds, since we usually have more than four points in the r direction. If the convection is not negligible, then the condition (5.8) would be less severe. Taking into account the convection in the logarithmic region it can be shown that

$$\frac{R}{h_z} > \frac{2.85 + \ell n(E h_z^+)}{1 + \ell n(E\ h_z^+)} \qquad (5.9)$$

The ratio of the rate of convergence of the coupled to the non-coupled k-ε system can be shown to be approximately, for $\sigma_z = \sigma_r = 1$,

$$\frac{R_C}{R_S} \approx 1 + \frac{2.85 + \ell n(E\ h_z^+)}{\frac{Re_c}{4} + 21.8\ \ell n(E\ h_z^+) + 9} \qquad (5.10)$$

which is about 1.15 ÷ 1.18 for practical solutions.

5.3 Application of the Turbulent Wall Boundary Conditions

The wall boundary conditions for the turbulent field solutions are not applied implicitly in the computational procedure. After every iteration the near-wall values are updated as follows:

At point 1, which is a distance h away from the wall (see Fig. 4.2 or 4.4), the new values of all the field quantities are known after the nth iteration. Then the following steps are taken:

(i) solution of the non-linear equation for v^*/Re from eq. (4.53a),

(ii) obtaining $\omega^+(y=0)$ from (4.53b) and replacing the old Ω on the wall by the new ω/r_w,

(iii) solving eq. (4.53c,d) for k^+ and ε^+ and replacing ε_w, ε_1 and k_1

Similar steps are taken for evaluating the temperature gradients on the wall for every iteration of the energy equation. The above explicit treatment of the turbulent boundary conditions may be shown to be stable by plotting on a curve of $(-\omega^+)$ vs. ψ^+ some of these explicit iterations as in Fig. 6.9. Since this curve exhibits convergence (the limit $\psi^+ \to \infty$ exists), and since the system of equations demands increasing ψ^+ values for increasing ω^+ values, this procedure is stable.

6. COMPUTATIONAL RESULTS AND COMPARISON WITH PREVIOUS WORK

6.1 Grid Development

A variable spacing grid was chosen to allow for more grid points in the regions of large gradients which are located as part of the solution process in order to obtain an accurate solution with a small total number of points. Since the large gradients of velocity, as well as those of turbulence quantities occur near the solid walls, more points will be located in the wall regions. An analytic distribution is preferred in order to minimize the effect of the $(\sigma - \frac{1}{\sigma})$ coefficient in the finite difference forms in Chapter 4. Since we are mostly interested in turbulent flows, a geometric variation of the grid spacing might be a good choice since the mean flow velocities are almost linear on the geometric transformation coordinates.

Figure 6.1 illustrates the grid in the r direction. The inner cylinder is located at $j = N_1$ where the total number of points in the r direction are N. The radius of the point Q has the value of $\frac{1}{2}(1+r_2)$, with the integer point j. It is assumed that

$$\begin{aligned} h_r &= a\, q_1^{k_2} \qquad 0 \le k_1 \le N_1 - 1 \quad \text{for} \quad j \le N_1 \\ h_r &= a\, q_2^{k_2} \qquad 0 \le k_2 \le N_2 - 1 \quad \text{for} \quad N_1 \le j \le N_1 + N_2 - 1 \end{aligned} \tag{6.1}$$

(see Fig. 6.1). The points $N_1 + 1$ and $N_1 - 1$ both are the same distance from the inner cylinder wall. The geometrical coefficients

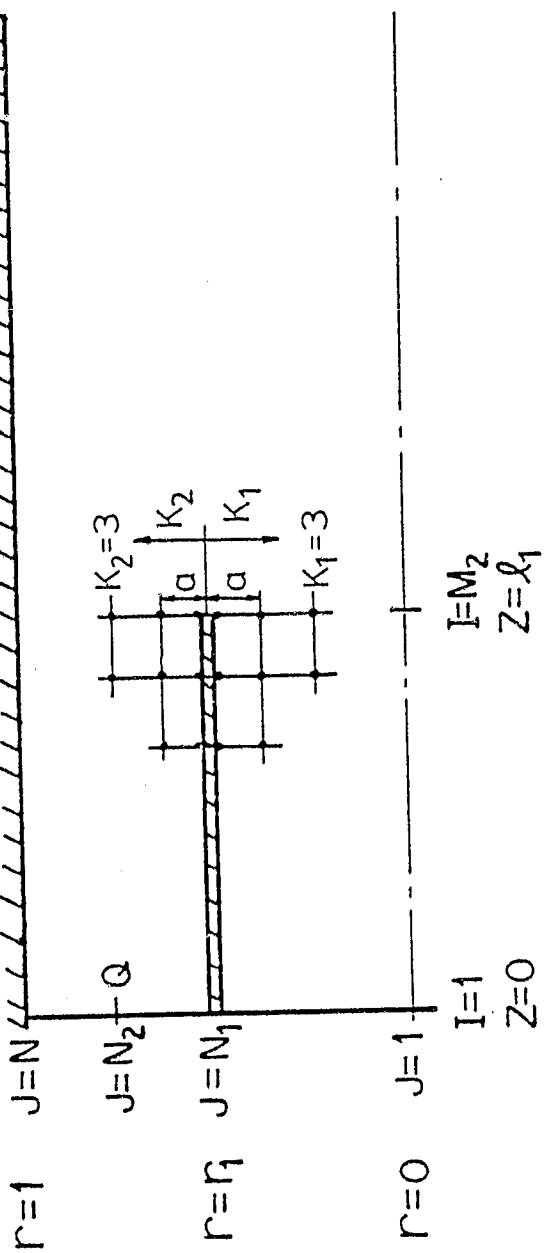

FIGURE 6.1: GRID GENERATION PARAMETERS

q_1 and q_2 should fulfill the following relations

$$r_1 = \frac{a}{q_1 - 1}\left(q_1^{N_1} - 1\right)$$

$$r_1 + 1 = 2\,\frac{a}{q_2 - 1}\left(q_2^{N_2} - 1\right) \qquad (6.2)$$

For a given "a", equations (6.2) will give q_1 and q_2. Usually "a" is determined beforehand, i.e., to give the number of points we desire to be located in the boundary layer region, or to guarantee that this point is in the logarithmic region.

Although this non-constant spacing grid is an attempt to raise the efficiency of the calculation (by using a smaller number of grid points) it is still far from the optimal grid. This is because in the core region far downstream from the inner cylinder trailing edge, there are many more grid points than are necessary to trace the fairly smooth variation of the variables. This is however, possibly the best transformation that can be applied to this field without using much more complicated curvilinear coordinate transformations obtained from differential mappings. A sample of the coordinate system around the trailing edge of the inner cylinder is given in Fig. 6.2. Here $q_1 = 1.38$ and $q_2 = 1.3$ for $r_1 = 0.362$, and the geometric series factor in the z direction is 1.8.

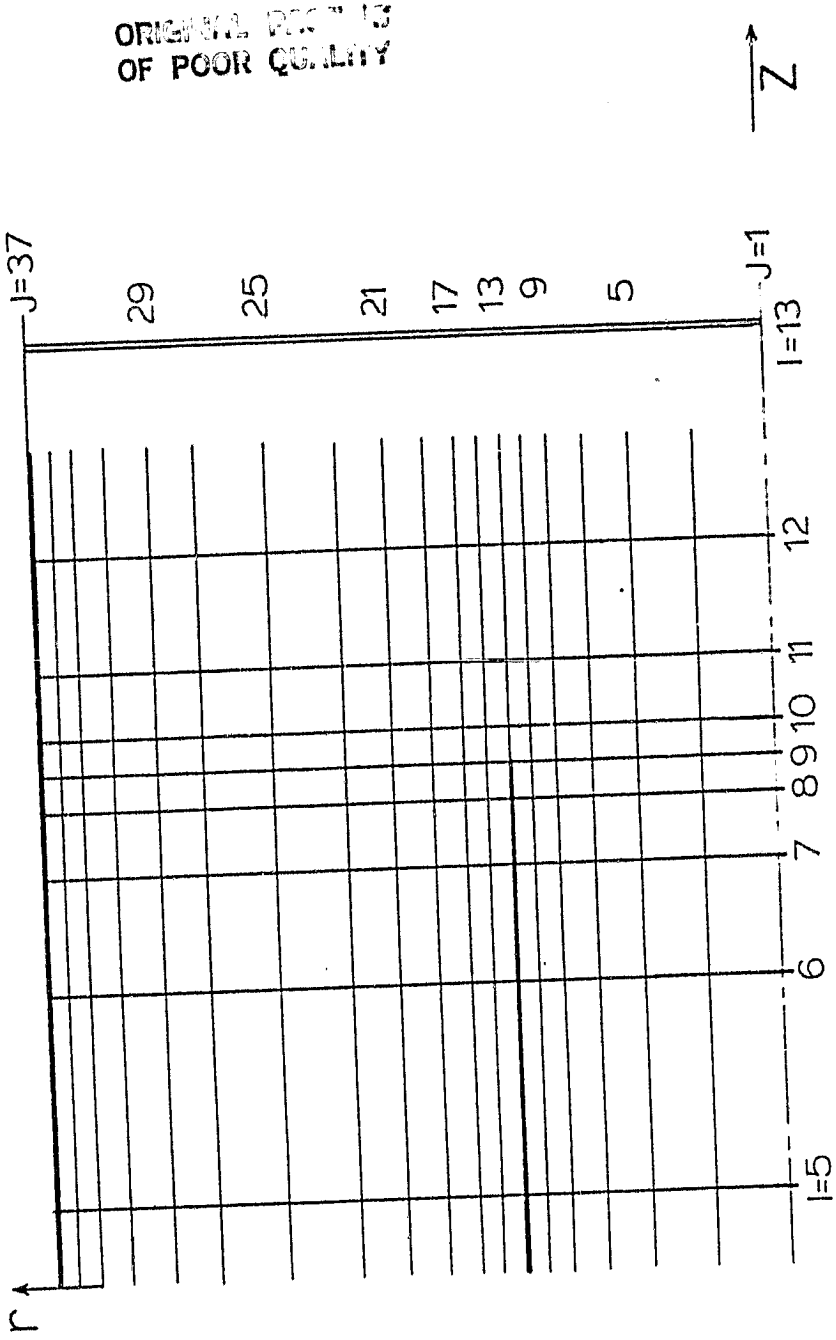

FIGURE 6.2: A SAMPLE GRID MESH

6.2 The Laminar Field

A program for obtaining solutions for the mixing of a confined coaxial flow was developed, based on the numerical methods presented. The validity of the numerical procedure was checked by comparison with other results in the literature. It was found that the present procedure yields results for an entrance region flow with an initial plug profile entering a pipe that varies by 0.1% from analytical results.[29]

It is convenient to define the ratio of the mean velocity of the outer jet to the mean velocity of the inner jet as a parameter

$$\frac{U_2}{U_1} = \frac{\psi_2 - \psi_1}{1 - r_1^2} \Big/ \frac{\psi_1}{r_1^2} \tag{6.3}$$

as well as the mean Reynolds number

$$Re_m = \psi_2 \cdot Re \tag{6.4}$$

Another check was made for confined jet mixing using the same field parameters as others:[30]

$$\frac{U_2}{U_1} = 1.17 \; ; \quad Re_m = 496 \; ; \quad r_1 = 0.5$$

The maximum discrepancy from the analytical results was about 1%. Here a 41 x 31 grid was used with $\ell_1 = 5$ and $\ell_2 = 15$. The second order accuracy of the scheme was verified with $\ell_2 = 6$ chosen as the outlet section to impose the parabolic conditions.

Predictions of the intensity of the reverse flow, $-\psi_{min}/\psi_m$ for $r_1 = 0.5$ and $U_2/U_1 = 20$, are described in Fig. 6.3 for fully developed inlet profiles. There is not much difference between the $z_1 = 3$ and the $z_1 = 5$ results. The results were not stable above $Re_m = 3200$. In the range of $3200 < Re_m < 4200$ the error in the iteration procedure did not grow, but it did not decrease either. Above a mean Reynolds number of ~5000 the iteration procedure blows up. The zone of separation is a function of Re_m and U_2/U_1. In Fig. 6.4 the locations of the separation and the reattachment points as functions of Re_m are described. These results give the impression that perhaps there is an asymptotic bubble length as Re_m tends to infinity. For $r_1 = 0.5$ and $Re_m = 2000$, the laminar stream function is described in Fig. 6.5 for two cases: $U_2/U_1 = 50$ and $U_2/U_1 = 0.02$. In Fig. 6.6, the temperature field is described. The temperature difference between the inner and outer jet was the reference temperature. The temperatures rise on the axis of symmetry is of the order of A/10 in eq. (3.13). The maximum rise in the temperature is near the end of flow field where the region of maximum heat generation is located.

6.3 The Turbulent Field

Calculations of the turbulent flow fields were carried out using experimental data for the inlet flow profiles. Unlike other work[31] the vorticity source term (3.30a) is not neglected since for $U_2/U_1 < 0.1$, $\nabla^2\nu$ is important in the high shear domains, especially near the dividing streamline and near

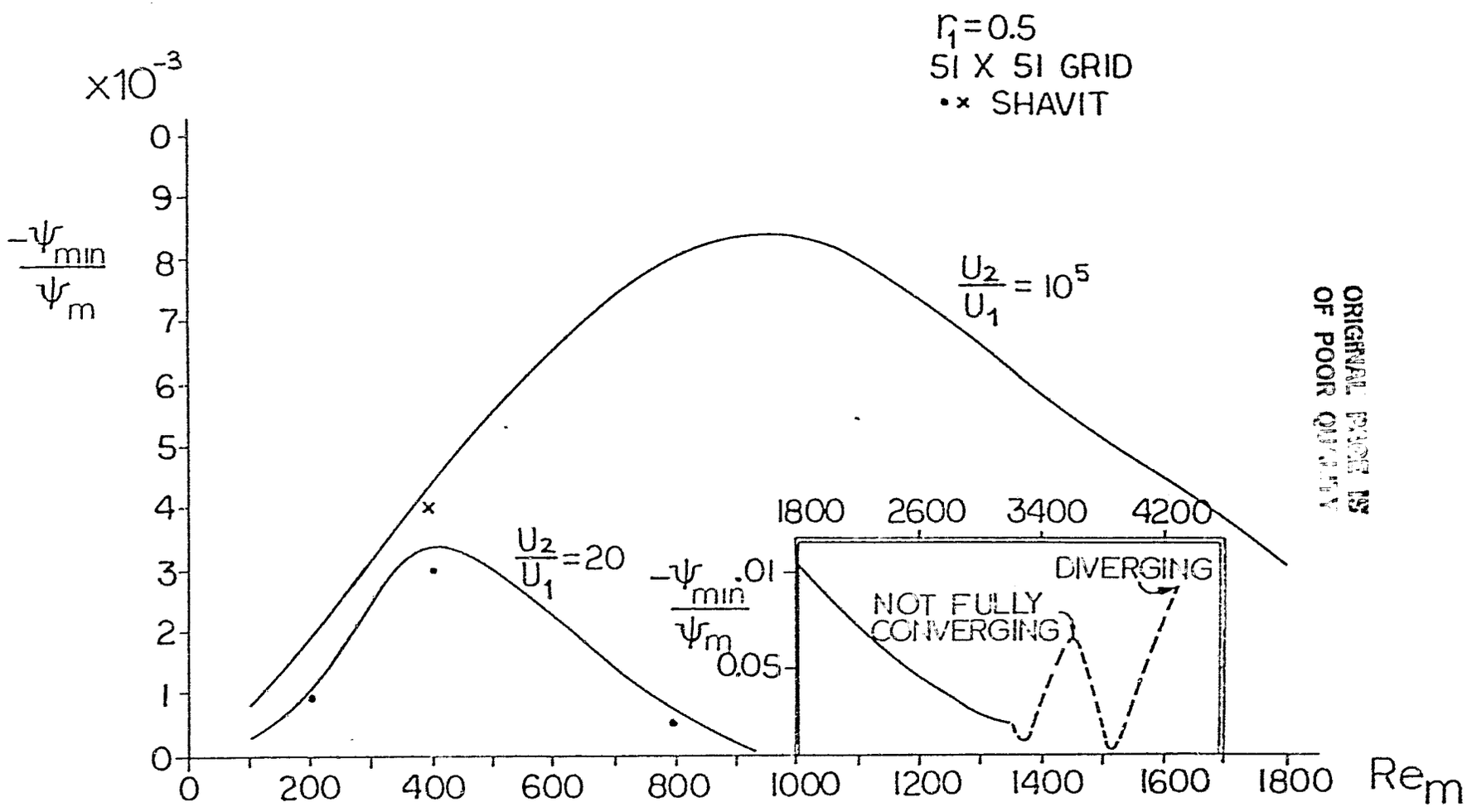

FIGURE 6.3: MAXIMUM RECIRCULATING MASS FLUX

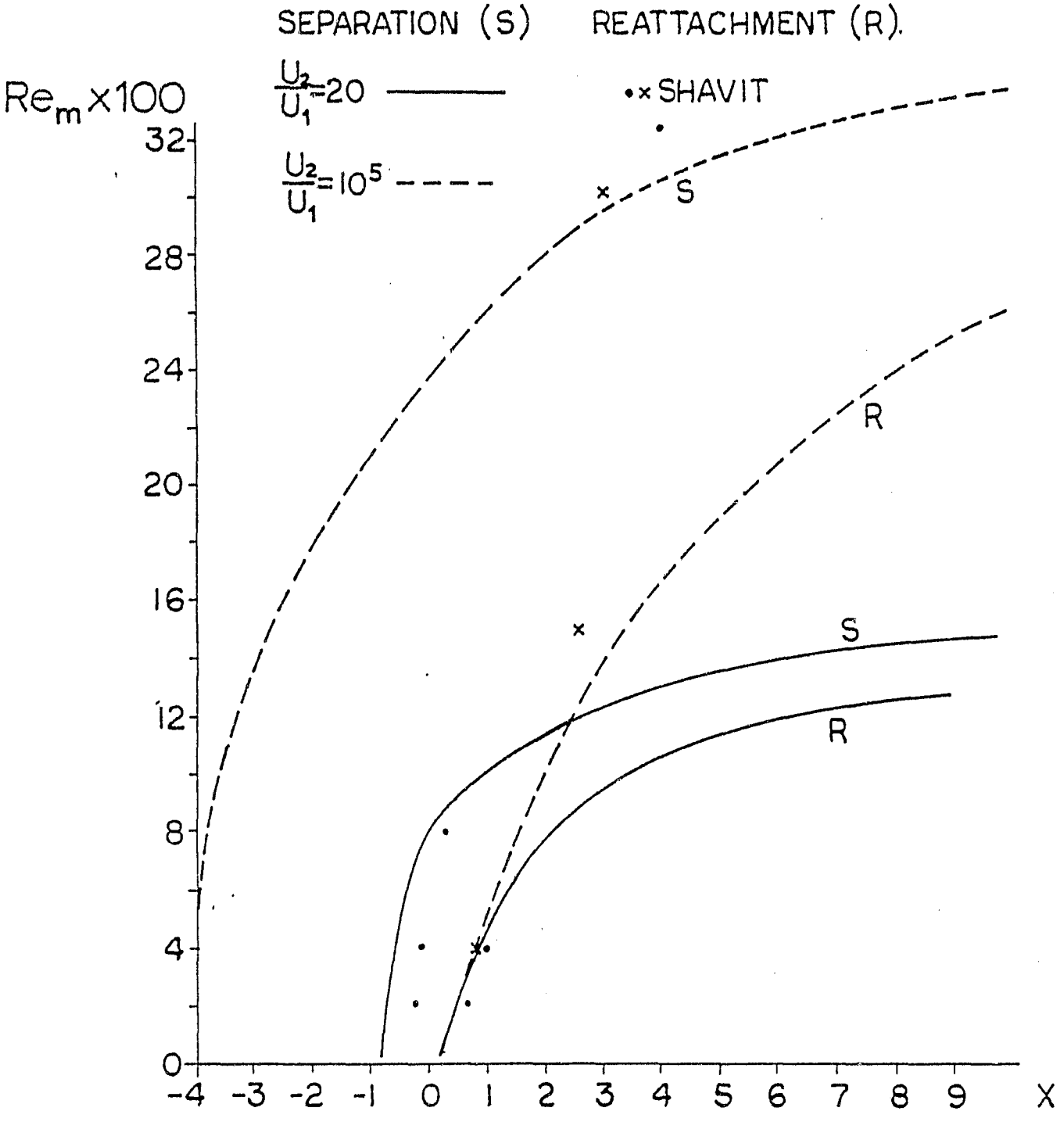

FIGURE 6.4: SEPARATION AND REATTACHMENT POINTS AS FUNCTION OF REYNOLDS NUMBER

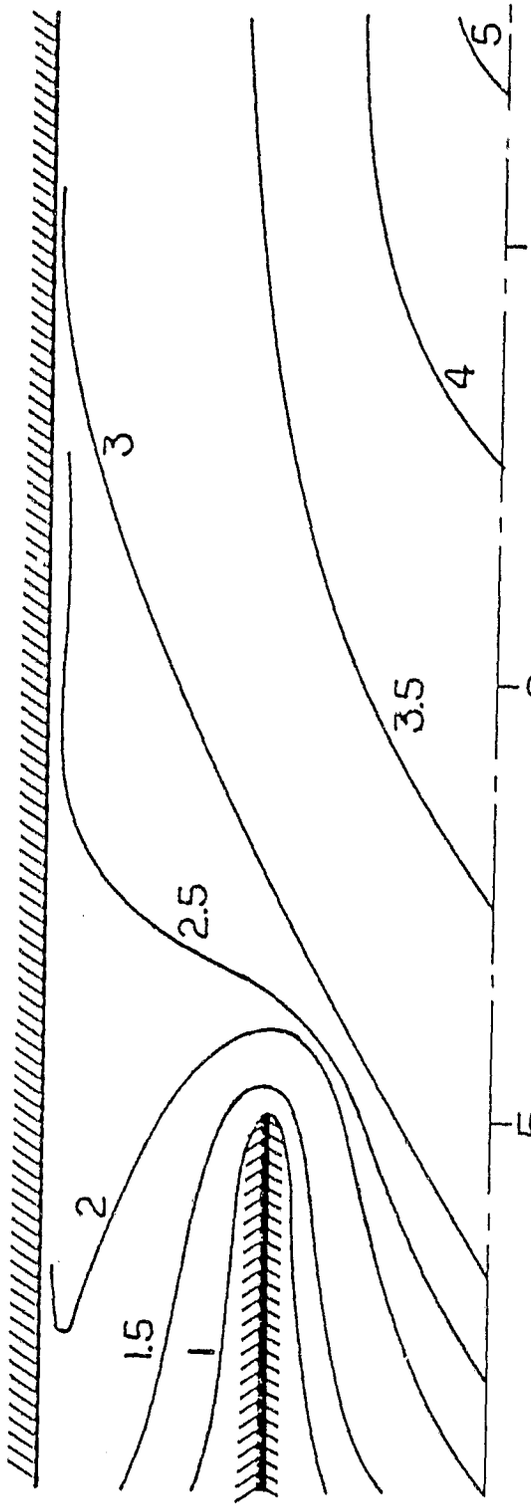

FIGURE 6.6: ISOTHERMS FOR $A=50$, $Re_m=1500$, $U_2/U_1=20$, $r_1=0.5$

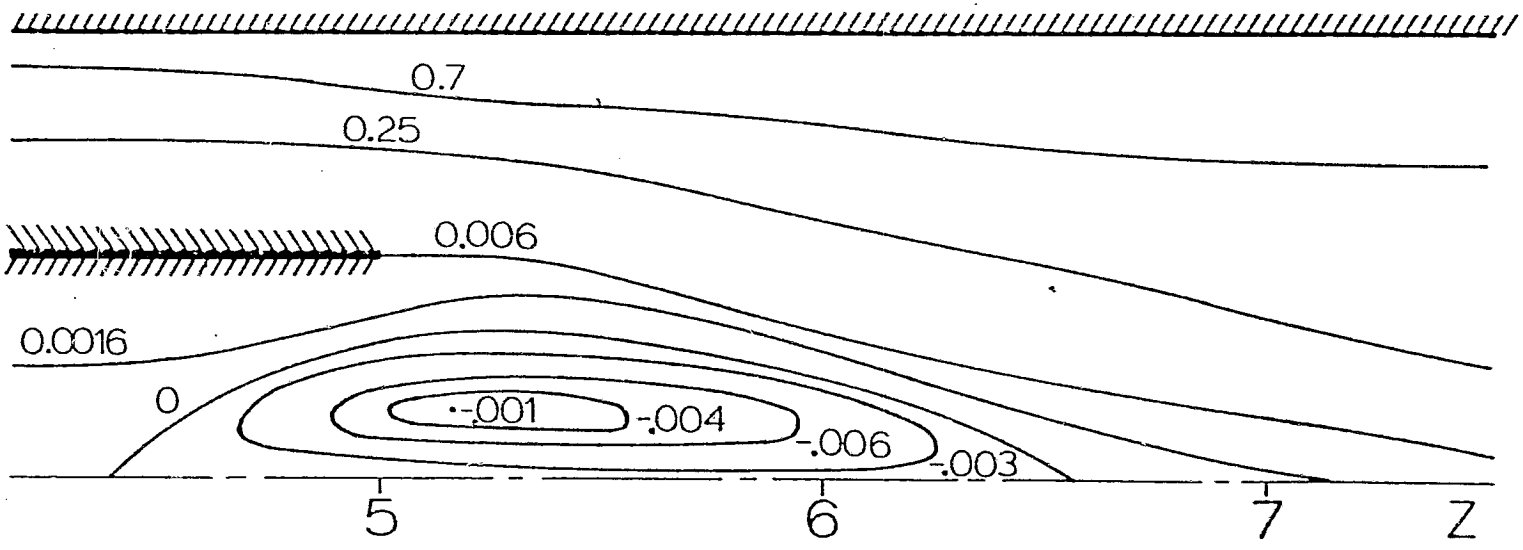

FIGURE 6.5b: STREAM FUNCTION CONTOUR LINES FOR $Re_m = 2000$, $r_1 = 0.5$, $U_2/U_1 = 50$

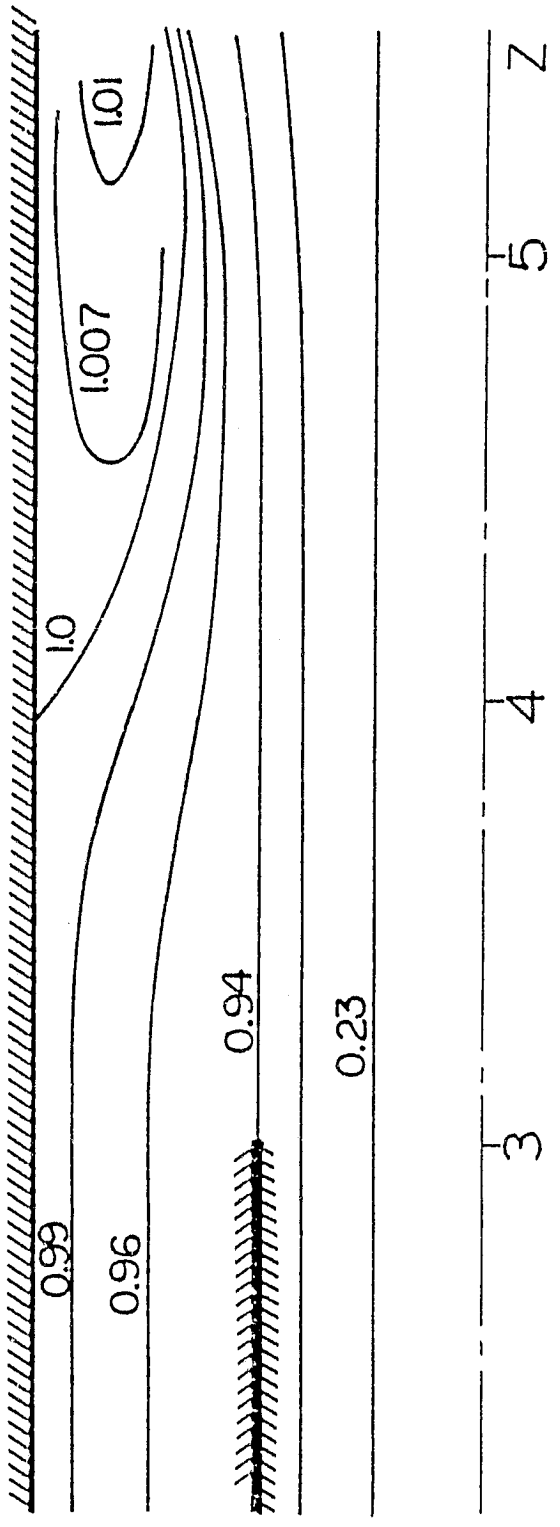

FIGURE 6.5a: STREAM FUNCTION CONTOUR LINES FOR Re_m=2000, r_1=0.5, U_2/U_1=.02

the walls in the viscous sub-layer zone where $\nabla^2 \nu \approx \eta^2$ (η is the normal to the shear layer direction). Similar to other works[32,33] the present study was done with $r_1 = 0.5$, Re = 72,000, and a pipe length, $L_2 = 20$. Predictions of the stream function and the turbulent kinetic energy for $U_2/U_1 = 40$ are described in Fig. 6.7. The temperature field of the present problem is shown in Fig. 6.8 for the constant A = 30. The effect of turbulent diffusion can be seen by the over-heating near the axis of symmetry at $z \approx 5$. That is due to the relative high ν_t. Due to a lack of experimental results for this field, the only check of the calculated results that was made is the global conservation of the variables. Mass was conserved to a 0.1% tolerance, while momentum and mean energy was conserved to a tolerance of 0.5%. The fact that the turbulent boundary conditions are, essentially, treated explicitly, reduces the rate of convergence. In Fig. 6.9, some of these explicit iterations are shown for a wall point at z = 3. Figure 6.10 demonstrates the difference in the convergence rate between a field where the point ahead of the outer cylindrical wall is located in the viscous sublayer, and a field where this point is located in the logarithmic region.

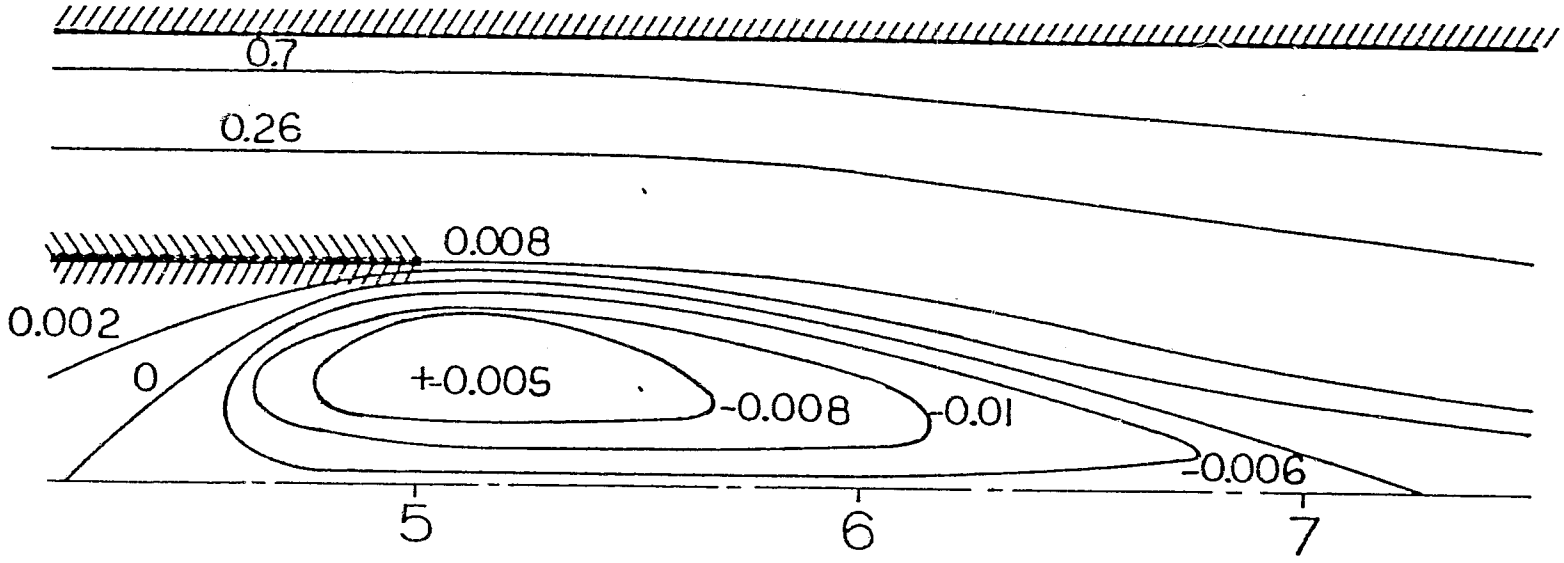

FIGURE 6.7a: STREAM FUNCTION CONTOURS FOR $Re_m = 7.2 \times 10^4$, $r_1 = 0.5$, $U_2/U_1 = 40$

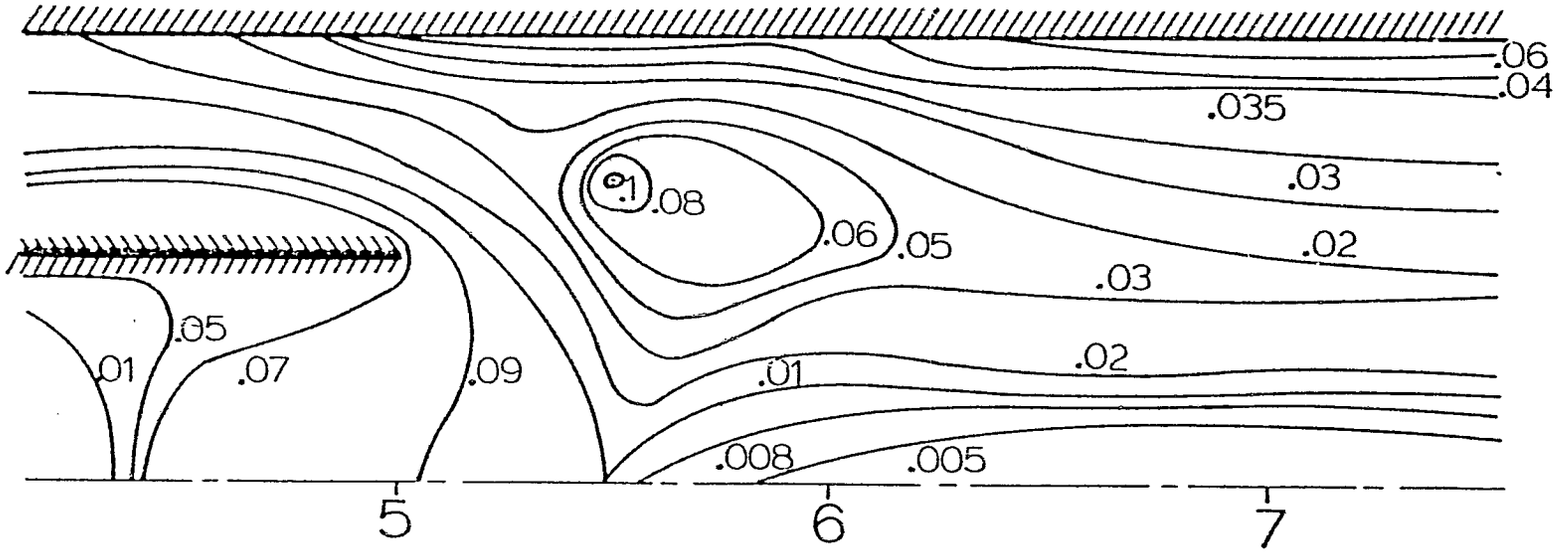

FIGURE 6.7b: TURBULENT KINETIC ENERGY CONTOURS FOR $Re_m = 7.2 \times 10^4$, $r_1 = 0.5$, $U_2/U_1 = 40$

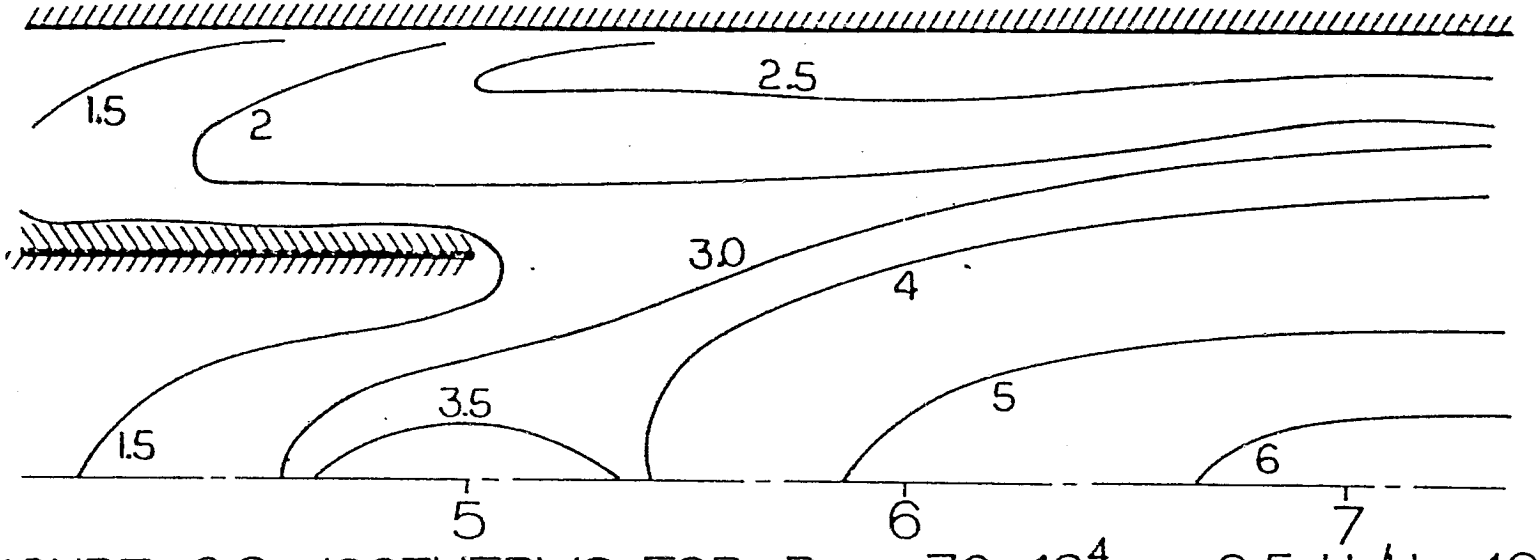

FIGURE 6.8: ISOTHERMS FOR $Re_m = 7.2 \times 10^4$, $r_1 = 0.5$, $U_2/U_1 = 40$

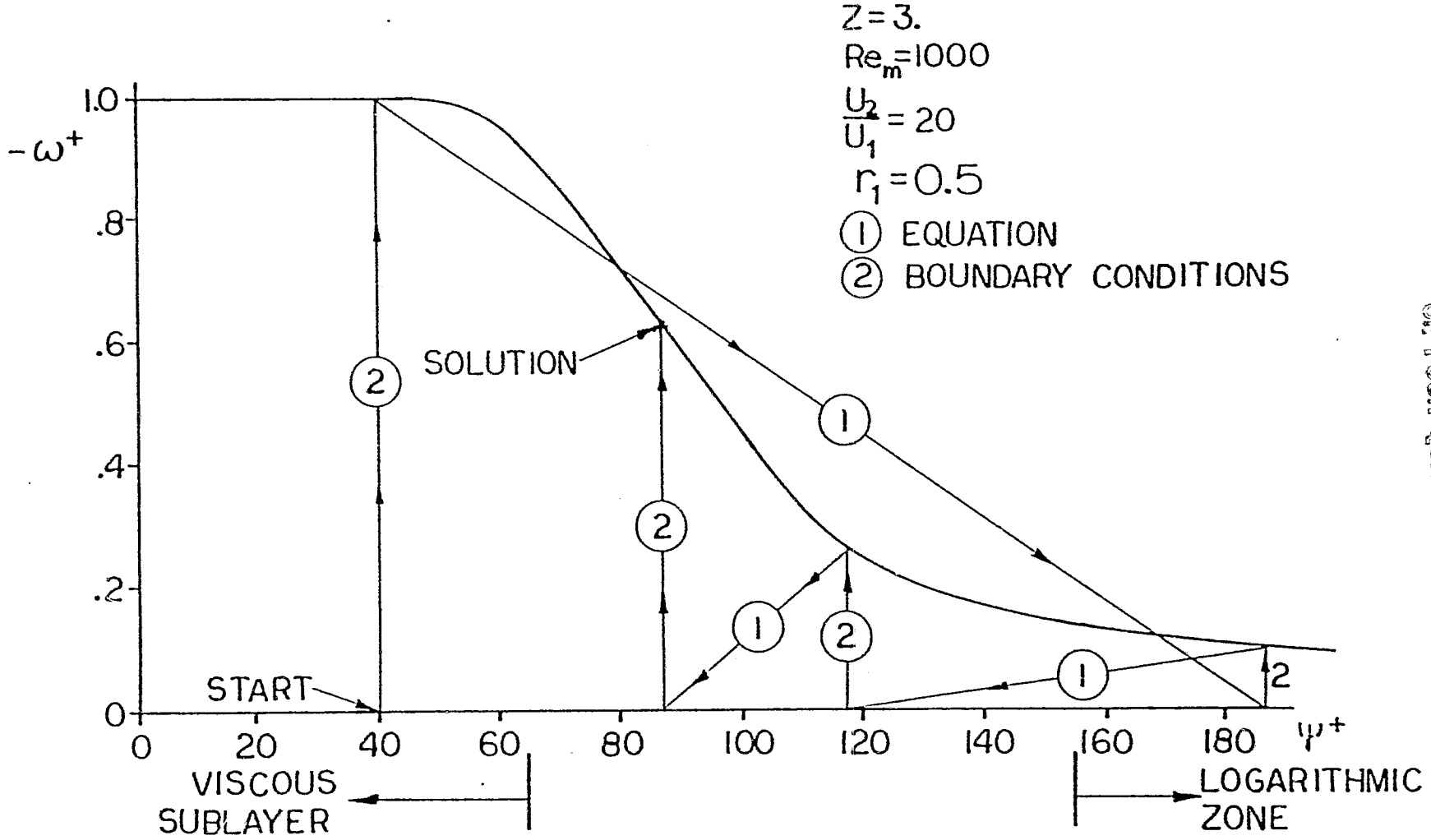

FIGURE 6.9: TURBULENT BOUNDARY CONDITIONS - MEAN FIELD INTERACTION, SOLVED ITERATIVELY

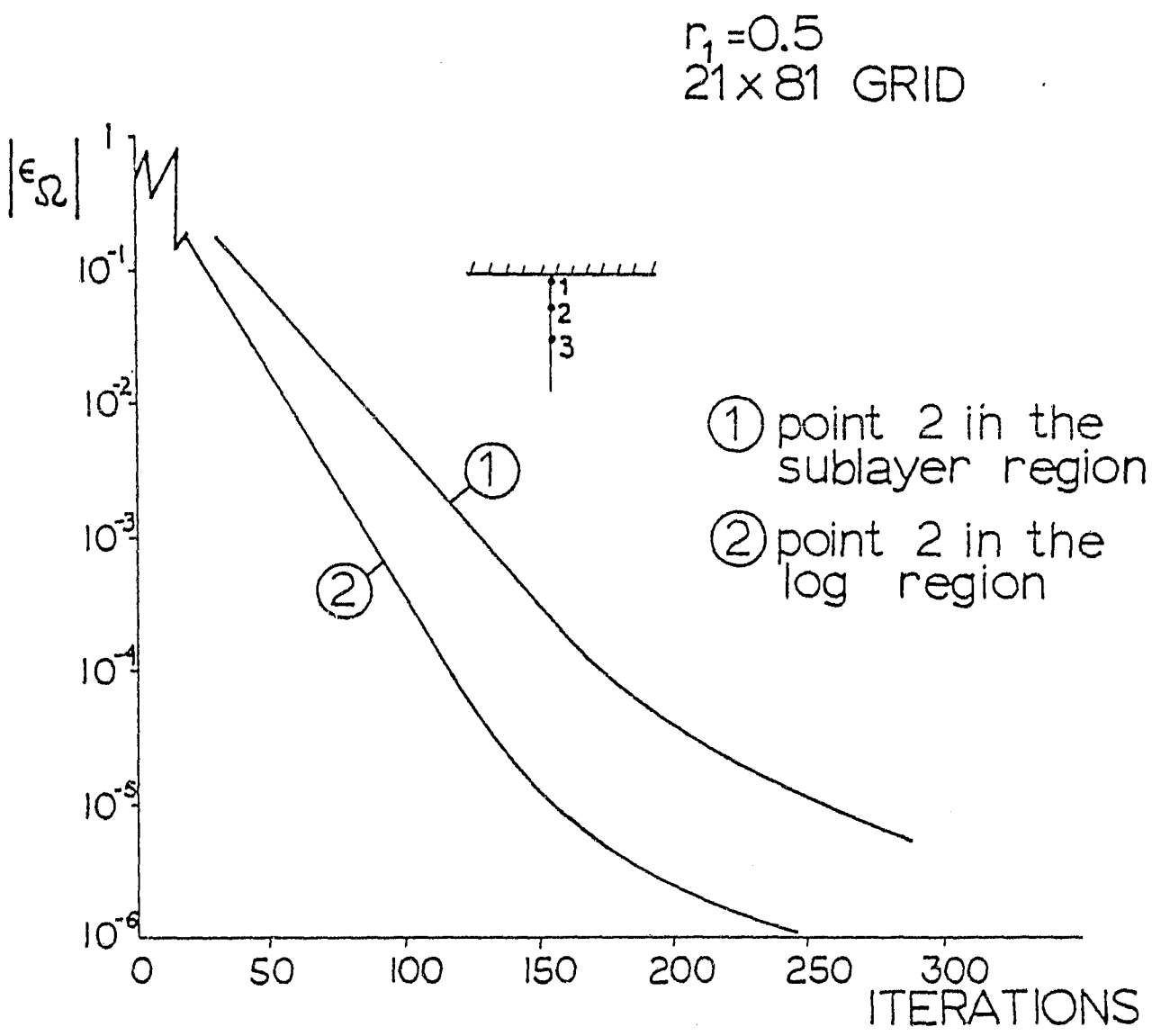

FIGURE 6.10: VARIATION OF THE ERROR IN Ω VS NUMBER OF ITERATIONS

7. CONCLUSIONS AND SUMMARY

This work is an attempt to solve numerically for the field of a two dimensional turbulent flow using a "two equation" type model for the turbulence. Since the flow field considered in this study is the incompressible confined turbulent mixing of two coaxial jets with internal heat generation, the mean stream function and mean vorticity were chosen as the flow variables. The turbulence effects were represented with the k-ε model. A conservative coupled-variable finite-difference scheme was employed. The finite-difference algebraic equations were solved iteratively by successive block line relaxation. Conditions for obtaining stable turbulent solutions were formulated. The double value of the vorticity and the poorly defined variation of the turbulent variables at a sharp corner were treated through the generation terms.

Although the coupling between ψ-Ω equations and k-ε equations tend to increase the convergence of the solution, the explicit form of the boundary conditions tend to decrease the rate of convergence compared to that of the laminar field. Since the gradients of all the variables in the logarithmic region near a wall is much smaller than they are in the sublayer region, the rate of convergence there is much faster. The downstream face boundary condition, $\partial^2/\partial z^2 = 0$, is the correct one to be applied for the so-called "fully-developed turbulent flow" condition since applying a $\partial/\partial z = 0$ condition contradicts

the boundary conditions on the wall. Applying such a boundary condition to a turbulent flow field can cause erroneously large turbulent diffusion coefficients in the field. There is no effect of the inlet conditions if they are applied far enough upstream from the trailing edge of the inner cylinder (~ 3 to 5 R).

References

1. Jones, W.P. and Launder, B.E., (1972), "The Prediction of Laminarization with a 2-Equation Model of Turbulence," Int. J. of Heat and Mass Transfer, 15, pp. 301.
2. Launder, B.E. and Spalding, D.B., (1974), "The Numerical Computation of Turbulent Flows," Comp. Meth. App. Math. and Eng., 3, pp. 269-289.
3. Rosseland, S., (1931), in Hottel, H.C., and Sarofim, A.F., (1967), Radiative Heat Transfer, McGraw-Hill Book Company.
4. Spalding, D.B., (1972), "A Novel Finite Difference Formulation for Differential Expressions Involving Both First and Second Derivatives," International Journal Numerical Methods in Engineering, 4, pp. 551.
5. Patankar, S.V. and Spalding, D.B., Heat and Mass Transfer in Boundary Layers, 2nd Edition, Intertext Books, London.
6. Schlichting, H., (1968), Boundary Layer Theory, 6th Edition, McGraw-Hill.
7. Launder, B.E. and Spalding, D.B., (1972), Mathematical Models of Turbulence, London.
8. Kolmogorov, A.N., (1942), "Equations of Turbulent Motion in an Incompressible Fluid," Isv. Akad. Nauk, USSR, VI, 1.2, pp. 56-58.
9. Roache, P.J., (1972), "Computational Fluid Dynamics," Hermosa, Albuquerque, NM.
10. Piacsek, S.A., (1968), "Some Problems in Numerical Solution of Three-Dimensional Incompressible Fluid Flows," Proc. 7th Symp. Naval Hydrodyn., Rome, Italy, Aug. 25-30; ONR, Dept. of the

Navy, DR-148, pp. 1616-1618.

11. Roache, P.J., (1975), Recent Developments and Problem Areas in Computational Fluid Dynamics, Lecture Notes in Mathematics 461, in "Computational Mechanics," pp. 195-256, Springer, Berlin.

12. Staff of Langley Research Center, (1975), "Numerical Studies of Incompressible Viscous Flow in a Driven Cavity," NASA SP-378.

13. Richtmeyer, R.D. and Morton, K.W., (1957), "Difference Methods for Initial-Value Problems," 2nd Edition, Interscience.

14. Oberkampf, W.L., (1976), "Domain Mappings for the Numerical Solution of Partial Differential Equations," Int. J. Numer. Methods Eng., 10, pp. 211-223.

15. Fanning, A.E. and Mueller, T.J., (1973), "Numerical and Experimental Investigation of the Oscillating Wake of a Blunt-Base Body," AIAA Journal, 11, 11, pp. 1486-1491.

16. Roache, P.J. and Mueller, T.J., (1970), "Numerical Solutions of Laminar Separated Flows," AIAA Journal, 8, 3, pp. 530-538.

17. Thoman, D.C. and Szewczyk, A.H., (1971), Time-Dependent Viscous Flows Over a Circular Cylinder, Ibid., pp. 76-86.

18. Torrance, K. et al., (1972), "Cavity Flows Driven by Buoyancy and Shear," J. Fluid Mech., 51, 2, pp. 221-231.

19. Gentry, R.A., Martin, R.E. and Dayly, B.J., (1966), "An Eulerian Differencing Method for Unsteady Compressible Flow Problems," J. Comput. Phys., 1, pp. 87-118.

20. Khosla, P.K. and Rubin, S.G., (1974), "A Diagonally Dominant Second-Order Accurate Implicit Scheme," Computers and Fluids, 2, pp. 207-229.

21. Khosla, P.K. and Rubin, S.G., (1979), "Navier-Stokes Calculations with a Coupled Strongly Implicit Method, Part I - Finite-Difference Solutions," 17th AIAA Aerospace Sciences Meeting, New Orleans, Paper 79-011.

22. Hennecke, D.K., (1970), "Flow and Heat Transfer in a Rotating Cavity with Axial Through Flow," Ph.D. Thesis, University of Minnesota.

23. Hanjalaic, K., and Launder, B.E., (1976), "Contribution Towards a Reynolds Stresses Closure for Low-Reynolds Number Turbulence," J. of Fluid Mech., 74, 4, pp. 593-610.

24. Chen, C.P., (1973), "Determination Experimentale Du Nombre de Prandtl Turbulent pres d'une Pario Lisse," Int. J. Heat Mass Transfer, 16, pp. 1849-1862.

25. Rotta, J.C., (1964), Int. J. Heat Mass Transfer, 7, pp. 215.

26. Ludwieg, H., (1956), Z. Flugwiss, 4, pp. 73.

27. Johnson, D.S., (1959), J. Appl. Mech., 26, pp. 26.

28. Baker, R.J. and Launder, B.E., (1974), "The Turbulent Boundary Layer with Foreign Gas Injection. I - Measurements in Zero Pressure Gradient. II - Prediction and Measurements in Severe Streamwise Pressure Gradients," Int. J. Heat Mass Transfer, 17, pp. 275-291 and 293-306.

29. Sparrow, E.M., Lin, S.H. and Lundgren, T.S., (1964), "Flow Development in Hydrodynamic Entrance Region of Trobes and Ducts," Phys. of Fluids, pp. 338-346.

30. Ghia, K.N., Torda, T.P., and Lavan, Z., (1968), "Laminar Mixing of Heterogeneous Axisymmetric Coaxial Confined Jets," NASA CR-72480.

31. Atkins, D.J., Maskell, S.J. and Patrick, M.A., (1980), "Numerical Prediction of Separated Flows," Int. J. for Num. Meth. in Eng., 15, pp. 129-144.

32. Ha Minh, H. and Chassaing, P., (1979), "Perturbations of Turbulent Pipe Flow," in Turbulent Shear Flows I, Durst, F., Launder, B.E., Schmidt, F.W. and Whitelaw, J.H., editors, Springer-Verlag, pp. 178-197.

33. Chaturvedi, M.C., (1963), "Flow Characteristics of Axi-symmetric Expansions," J. Hydraulics Div., pp. 61-62.

34. Shavit, G., (1970), "Analytical and Experimental Investigations of Laminar Mixing of Homogeneous and Hetrogeneous Jets in a Con. Tube," Ph.D. Thesis, Illinois Institute of Technology.

35. Hirsh, R.S. and Rudy, D.H., (1974), "The Role of Diagonal Dominance and Cell Reynolds Number in Implicit Difference Methods for Fluid Mechanics Problems," Journal of Computational Physics, 16, 3, pp. 304-310.

NOMENCLATURE

C	concentration function
C_1, C_2, C_μ	k-ε model coefficients
D	partial differential operator defined in eq. (3.26)
D	mass diffusion coefficient
G	turbulent energy production
k	turbulent energy
L	typical axial length
p	pressure
Pr	temperature Prandtl number
Q	mass flux
r	radial direction and coordinate
R	radius
R_c, R_s	rate of convergence
R_d	radiation number
Re	Reynolds number
Re_m	mean Reynolds number
R^z, R^r	truncation error
S	source term
Sc	Schmidt number
S_T	heat generation rate
T	temperature
u	axial velocity
v	radial velocity
z	axial direction and coordinate

α_r	the thermal radiative diffusivity
γ	integer to choose the right differencing direction
ε	turbulent energy dissipation
λ	thermal conductivity
μ	laminar viscosity coefficient
μ_t	turbulent viscosity coefficient
μ_{eff}	the effective viscosity coefficient
ν	kinematic viscosity coefficient
σ_k	turbulent energy Prandtl number
σ_ε	dissipation Prandtl number
τ	stress tensor
ψ	stream function
ψ_m	maximum stream function
ω	vorticity
Ω	ω/r

Indexes

1	inner cylinder
2	outer cylinder
eff	effective
i,j	tensorial indices
ℓ	laminar
r	radiation
t	turbulent